ORIGINAL ARTICLE

Word Count: 5747

Oscillating Steady-State Imaging (OSSI): A Novel Method for Functional MRI

Shouchang Guo[1] | **Douglas C. Noll**[2]

[1]Department of Electrical Engineering and Computer Science, University of Michigan, Ann Arbor, MI 48109, USA

[2]Department of Biomedical Engineering, University of Michigan, Ann Arbor, MI 48109, USA

Correspondence
Shouchang Guo, Functional MRI Laboratory, 1073 BIRB, 2360 Bonisteel Blvd, Ann Arbor, MI 48109-2108.
Email: shoucguo@umich.edu

Funding information
This work was supported by National Institute of Biomedical Imaging and Bioengineering (NIBIB) and National Institute of Neurological Disorders and Stroke (NINDS) through grants R01 EB023618 and U01 EB026977.

Purpose: Signal-to-noise ratio (SNR) is crucial for high-resolution fMRI, however, current methods for SNR improvement are limited. A new approach, called Oscillating Steady-State Imaging (OSSI), produces a signal that is large and T_2^*-weighted, and is demonstrated to produce improved SNR compared to gradient echo (GRE) imaging with matched TE and spatial-temporal acquisition characteristics for high-resolution fMRI.

Methods: Quadratic phase sequences were combined with balanced gradients to produce a large, oscillating steady-state signal. The quadratic phase progression was periodic over short intervals such as 10 TRs, inducing a frequency-dependent phase dispersal. Images over one period were combined to produce a single image with effectively T_2^*-weighting. The OSSI parameters were explored through simulation and phantom data, and 2D and 3D human fMRI data were collected using OSSI and GRE imaging.

Results: Phantom and human OSSI data showed highly reproducible signal oscillations with greater signal strength than GRE. Compared to single slice GRE with matched TE and spatial-temporal resolution, OSSI yielded more activation in visual cortex by a factor of 1.84 and an improvement in temporal SNR by a factor of 1.83. Voxelwise percentage change comparisons between OSSI and GRE demonstrate a similar T_2^*-weighted contrast mechanism with additional T_2'-weighting of about 15 ms immediately after the RF pulse.

Conclusion: OSSI is a new acquisition method that exploits a large, oscillating signal that is T_2^*-weighted and suitable for fMRI. The steady-state signal from balanced gradients creates higher signal strength than single slice GRE at varying TEs, enabling greater volumes of func-

tional activity and higher SNR for high-resolution fMRI.

KEYWORDS

Oscillating Steady-State Imaging (OSSI), T_2^*-weighting, functional MRI, BOLD contrast, high SNR, high-resolution

1 | INTRODUCTION

Because the signal-to-noise ratio (SNR) in MRI is proportional to voxel volume, and the functional units of the brain are on the order of 1 mm, high SNR is required for functional MRI (fMRI) of these small brain structures. Many common methods for improving SNR have already been well-used, but now face limitations. For example, extending readouts increases sensitivity to off-resonance distortions, and increasing the number of coils in a head array suffers from diminishing returns as coil elements get smaller, particularly for deep brain structures. One can also enhance SNR by going to higher field systems, but this requires a costly investment. Thus, there is a compelling need for alternative approaches to improving the SNR in fMRI.

Functional MRI using the blood oxygenation (BOLD) effect has been based on T_2^*-weighted gradient echo (GRE) imaging from its inception and has commonly been implemented using single-shot fast imaging methods like echo-planar imaging (EPI) or spiral imaging. There has also been some work on acquisition using steady-state methods. These include T_2^*-weighted, 3D GRE acquisitions of several variations [1, 2] and short TR, fast recovery (STFR) sequences that preserve magnetization through principles of driven equilibrium [3]. There are also variants of balanced steady-state methods like balanced steady-state free precession (bSSFP, also known as True FISP, FIESTA, bFFE), such as transition-band bSSFP [4, 5], have exploited shifts in resonant frequency associated with changes in blood oxygenation. At the same time, blood oxygenation changes have also led to observable signal changes using passband bSSFP resulting from changes in T_2 directly and from diffusive effects around small vessels [6, 7, 8].

Standard implementations of bSSFP use constant excitation phase or a linear phase sequence for RF pulses. In this work we use a similar balanced-gradient pulse sequence, but with quadratic phase sequences, which is equivalent to a linearly sweeping frequency. Since the frequency response is periodic in the frequency domain, a frequency sweep will lead to periodic signal oscillation. We note that if the gradients are not balanced (e.g. gradient spoiled), the quadratic phase sequence will lead to a RF-spoiled gradient echo acquisition, provided that the sweep rate is sufficiently fast. Also, if the quadratic phase sequence is sufficiently slowly evolving, then the balanced-gradient acquisition leads to contrast that is very similar to the standard bSSFP contrast though the response slowly shifts over time. In this work, we explore a novel domain using balanced-gradients but with a quadratic phase sequence that is rapid, having a period on the order of 10 TRs, which leads to an oscillatory signal. We refer to this approach as Oscillating Steady-State Imaging (OSSI). We show that the OSSI signal is large compared to Ernst angle GRE imaging and further show that the OSSI signal is sensitive to changes in T_2^*, making it suitable for high-resolution fMRI. We distinguish our approach using quadratic phase sequences from other oscillatory steady states resulting from sequences

of alternating patterns of phase [9, 10], which have a different contrast.

In this work, we demonstrate a novel fMRI acquisition method that has the potential to improve the SNR over GRE with matched TE and spatial-temporal acquisition characteristics. It focuses on a unique oscillating steady-state source of signal that is large and T_2^*-weighted, and we explore its signal properties in both simulation and experimental studies.

2 | THEORY

2.1 | Oscillating Steady-State Imaging

Quadratic phase sequences in conjunction with a constant gradient dephasing is a well-recognized approach for establishing a spoiled steady state. The sequence is typically applied using the RF phase increment [11]

$$\phi(n) - \phi(n-1) = \psi_A n + \psi_B, \tag{1}$$

where ψ_A is commonly chosen to provide full cancellation of the transverse magnetization prior to the next RF pulse; typical values for spoiling are $\psi_A = 117°, 50°, 150°$, etc. The constant term, ψ_B, represents a constant frequency shift and is not important in most of these analyses. The linear phase increment is equivalent to a quadratic phase sequence, for example, $\phi(n) = \psi_A n^2/2$ is the same as in Equation (1) for the case of $\psi_B = -\psi_A/2$. In this work, we examine such quadratic phase sequences with balanced gradients, which maintains the steady-state components leading to stronger signals. This approach was proposed by Foxall [12] to implement bSSFP with T_2-like weighting whereby the frequency-dependent bands in image intensity slowly shifted over the acquisition. Foxall argued that bSSFP-like contrast would be preserved if the phase increment is kept small ($\psi_A < 3°$). We have observed that larger phase increments also leads to steady-state signals, however that the contrast is no longer similar to bSSFP contrast, but instead has contrast that is both T_2- and T_2'-weighted, and thus effectively T_2^*-weighted. With appropriate selection of ψ_A, the phase sequence can be made to be periodic with cycle length n_c by setting

$$\psi_A = \frac{2\pi}{n_c}. \tag{2}$$

This periodic sequence leads to oscillations in the steady-state signal with period $T_{OSSI} = n_c TR$. Maintenance of transverse components via a steady state tends to make the resultant signals T_2-weighted, while the different phases of different isochromats lead to T_2'-weighting. We note that Wang et al. [13] have similarly observed that quadratic phase RF pulses lead to frequency dependent phase variations and T_2^*-weighting.

The OSSI signals have a variety of interesting properties. Like bSSFP, the OSSI response is frequency dependent and the spectral properties are periodic with 1/TR in the frequency domain. Further, it can be shown that shifts in frequency will lead to signal being shifted in time. Specifically, a frequency shift of $1/T_{OSSI}$ will lead to the phase sequence being shifted by exactly one TR, which leads to the OSSI response being similarly shifted in time by one

TR. Note that a frequency shift of $1/T_{OSSI}$ is equivalent to $\Delta\psi_B = 2\pi/T_{OSSI}$. Frequency shifts that are not integer multiples of $1/T_{OSSI}$ will also have oscillatory behavior, but with slightly different temporal signal responses. Thus, different isochromats within an image will have unique time courses, each of which is periodic with T_{OSSI}, and depending on the frequency, these time courses will be shifted in time and/or have slightly different shape. The shifts in time for different isochromats induces a frequency dependent phase dispersal, effectively leading to T_2^*-like contrast. In order to produce a stable and usable time course for fMRI analyses, we commonly combine the n_c images for one period of the OSSI signal by some method, for example using root mean square (RMS) or 2-norm combination.

2.2 | OSSI Spin Behavior and Signal Simulation

OSSI spin behavior was examined using a Bloch equation simulator for spins having relaxation parameters similar to gray matter using the average of reported values [14] T_1 = 1433.2 ms and T_2 = 92.6 ms at 3T, and pulse sequence parameters TR = 15 ms with an excitation pulse length of 3.2 ms, number in phase cycle (n_c) = 10, and flip angle (FA) = 10°. The phase progression with n_c = 10 is equivalent to a spoiling seed of 36° for spoiled-GRE. An example of magnetization progression at steady state is shown for a spin with off-resonance -20 Hz in Figure 1, with the pattern repeating every n_c TRs. The signal intensity varies as magnetization moves towards and away from the center in (a), and the spin moves up and down in m_z (b). From Figure 1 (c), we can see that the magnitude of the OSSI signal right after the excitation at TE = 1.6 ms has a periodicity of n_cTR and is substantially larger than the spoiled GRE signal for the same parameters. Observe that off-resonance shifts of multiples of $1/T_{OSSI} = 1/(n_cTR)$ = 6.67 Hz lead to exactly the same temporal waveform with a shift of 1 TR in time. The isochromats in Figure 1 (c) and (d) cover a frequency range of 13.3 Hz and result in a 74.1° phase spread for the time point right after the RF pulse. Note that the phase between isochromats increases during the readout, which indicates increased T_2'-weighting, and there is no spin-echo signal formed at the center of readout, demonstrating a very different contrast mechanism compared to bSSFP. The observed phase accumulation is equivalent to a T_2'-weighting with an effective TE of 15.4 ms at beginning and 27.2 ms at the end of the readout interval, respectively.

Figure 2 (a) and (b) shows the magnitude and phase responses, respectively, as a function of time and frequency. In Figure 2 (c) and (d), one can see that frequency shifts that are not multiples of $1/T_{OSSI}$ lead to slightly different time courses in magnitude and phase. The duality between time and frequency is shown in Figure 2 (e) and (f). Here one can see that samples in frequency spaced at integer multiples of $1/T_{OSSI}$ will give exactly the same waveform as the time courses in Figure 2 (c) and (d), but reversed. More specifically, the OSSI signal M_T and the frequency response M_F have the following relationship

$$M_T(k \bmod n_c; f_0) = M_F\left(f_0 + \frac{1 - k \bmod n_c}{n_c\mathrm{TR}}\right), \tag{3}$$

where k is the TR number, and f_0 denotes the off-resonance frequency. From this expression, one can clearly see that the steady-state frequency response is the manifold on which the

time-course signals are found.

2.3 | Acquisition Parameter Optimization

In seeking to optimize the OSSI signal, there are a variety of measures of goodness. First, since we are interested in applying this method to functional MRI, we wish to maximize sensitivity to changes in the signal resulting from changes in T_2', normalized by the square root of imaging time. It is desirable to have smaller n_c as fewer TRs are needed to complete a single image, while longer TRs are preferred because they allow a longer time for acquisition. We also desire to maximize uniformity of the RMS combined OSSI signal as a function of frequency shifts smaller than $1/T_{OSSI}$.

To understand the impact of pulse sequence parameters on the OSSI signal, additional Bloch simulations were carried out. Figure 3 (a) shows the RMS combined signal intensity for OSSI as a function of n_c and flip angle for TR = 15 ms. Note that $n_c = 1$ corresponds to bSSFP, and for $n_c > 120$, the OSSI signal behaves similarly to bSSFP with a flat phase response (spin-echo-like contrast) over some range of off-resonance frequencies [12]. However, the bright signals in the upper left corner, bounded by the box, were somewhat unexpected and are the focus of this paper. Here, we examine a range of parameters with respect to sensitivity for fMRI studies and to undesired sources of signal variation.

Deoxygenation of blood at 3T primarily affects T_2' in tissue [15] and causes an approximately exponential decay $\exp(-t/T_2')$ of the BOLD signal. This effect can be modeled by averaging complex signals from a large number of spins with different off-resonance frequencies. When the number of spins is sufficiently large, there exists a Fourier relationship between $\exp(-|t|/T_2')$ and the probability density function of off-resonance frequency f, yielding the Cauchy distribution $G(f) = \gamma/(\pi(\gamma^2 + f^2))$, where γ is the scale parameter of the distribution and $T_2' = 1/(2\pi\gamma)$.

Therefore, to simulate the T_2^*-weighted signal of a voxel in the static dephasing regime, we generated complex OSSI signals from 2000 spins with off-resonance frequencies uniformly ranging from -150 Hz to 150 Hz, and calculated weighted sum of the complex signals. The weighting function is the Cauchy distribution $G(f)$ centered at a specific off-resonance frequency and using T_2' = 148.3 ms and 135.5 ms, corresponding to T_2^* of 57 ms and 55 ms given an underlying T_2 = 92.6 ms for gray matter, which were selected to model baseline and active conditions, respectively. The T_2^* difference represents a typical 1.9% signal change for a T_2^*-weighted GRE image with TE = 30 ms. The OSSI baseline and active signals were obtained by applying RMS combination to every n_c = 10 consecutive and non-overlapping time points of the T_2^*-weighted signals.

The OSSI signal of each spin was simulated using a range of parameters for TR, FA, and n_c. We varied two parameters while fixing the third parameter, and performed the simulation for at least 5 T_1s to ensure the signal was in steady state. The T_2^* sensitivity is defined by the difference of the active (T_2^* = 55 ms) and baseline (T_2^* = 57 ms) signals in units of M_0 either just after the RF pulse for spiral out acquisitions or just before the subsequent RF pulse for spiral-in acquisition. Figure 3 (b) and (c) gives the T_2^* sensitivity for a spiral-out acquisition (TE = 1.6 ms) as a function of different TRs and flip angles for n_c = 10, and different n_c and

flip angles at a fixed TR of 15 ms, respectively. Supporting Information Figure S1 (b) and (c) presents the same relationship for a spiral-in acquisition (TE = TR - 1.6 ms).

As noted above and shown in Figure 2, the OSSI pulse sequence is very frequency sensitive but for the use in fMRI an important question is the sensitivity of the combined (RMS over n_c points) signal vs. frequency. An example of this effect is the small difference between RMS combined signal of blue and red lines in Figure 2 (c). The combined signal is periodic in the frequency domain with $1/\mathrm{T_{OSSI}} = 1/(n_c\mathrm{TR})$, so we varied the central frequency offset over this range to obtain the signal variability due to field inhomogeneity. The variability was calculated by taking the maximum difference of the combined signals at different central frequencies. Figure 3 (d) and (e) give the frequency-dependent signal variability for the spiral-out acquisition as a function of different TRs and flip angles for n_c = 10, and different n_c and flip angles at a fixed TR of 15 ms, respectively. Supporting Information Figure S1 (d) and (e) shows the same relationship for a spiral-in acquisition. Note that the small central frequency dependent variations were averaged across $1/\mathrm{T_{OSSI}}$ for Figure 3 (a)-(c). To assess the T_2^*-weighting of OSSI in comparison to GRE using as long of a TE as possible (equivalent to a spiral-in acquisition), we plot the maximal T_2^*-weighted signal change vs. TR in the Supporting Information, Figure S2.

3 | METHODS

All the studies were performed on a 3T GE MR750 scanner (GE Healthcare, Waukesha, WI) with a 32-channel head coil (Nova Medical, Wilmington, MA). We implemented the OSSI pulse sequence using the vendor's standard pulse programming language, EPIC, and collected data with matched spatial and temporal resolutions using both OSS and GRE approaches.

3.1 | Phantom Experiments

To demonstrate the principles of OSSI, we collected images of the FBIRN phantom [16] (approximate T_1/T_2 = 530/60 ms) using both balanced and spoiled gradients. An oblique slice with FOV = 220 mm and slice thickness = 2.5 mm was acquired, and the voxel size = 6.29 $\times$ 6.29 $\times$ 2.5 mm^3. For OSSI, we chose TR = 15 ms, n_c = 10, FA = 10°, and a fully sampled single-shot spiral-out trajectory. The spoiled-GRE data were acquired with the same parameters, except for the addition of spoiling gradients and the use of a spiral-in readout to make the effective TEs of the two acquisitions more similar. Specifically, the OSSI spiral-out TE = 2.7 ms, which corresponds to an effective TE of 17.5 ms. To bring GRE TE closer to OSSI effective TE and to increase GRE T_2^*-sensitivity with the limited TR = 15 ms, we used GRE spiral-in TE = 11.2 ms. The number of time points = 100 with 10 s discarded acquisition prior to collecting data. Every n_c = 10 images (1 period of the oscillations) were combined pixel-wise using the 2-norm.

3.2 | Human Experiments

3.2.1 | 2D Human Studies

Human functional imaging studies were performed on 5 subjects using both OSSI and GRE methods with informed consent and IRB approval. The functional task was a left vs. right reversing-checkerboard visual stimulus (with 5 cycles of 20 s L/20 s R). The 2D sampling pattern for both GRE and OSSI was multi-shot (number of interleaves n_i = 8) fully sampled variable-density spirals with a densely sampled core (300 k-space points). A single oblique slice through visual cortex was selected with FOV = 220 mm and 2.5 mm slice thickness. The voxel size was $1.77 \times 1.77 \times 2.5$ mm^3 (matrix size 124×124). All the 2D images were reconstructed as 128×128 matrices. The experiments include 4 spiral-out acquisitions of 4 subjects and 4 spiral-in acquisitions of 4 subjects.

For the OSSI method, we chose TR = 15 ms, n_c = 10, and nominal FA = 10°. The OSSI effective TR for each spiral = 150 ms (TR $\cdot$ n_c) and the volume TR = 1.2 s (TR $\cdot$ n_c $\cdot$ n_i). For the GRE acquisition, we carefully matched spatial-temporal resolution of OSSI, each interleave was acquired with GRE TR = 150 ms, volume TR = 1.2 s (TR $\cdot$ n_i), and the Ernst flip angle FA = 27° to optimize SNR. The number of time points for OSSI was 1670 or 167 combined images, and the number of time points for GRE was 167 with no combination necessary, corresponding to the 200 s of the functional task. To establish the steady state, no data were collected for the first 10 s for both acquisitions. OSSI actual TE was set to minimum (TE = 2.7 ms) for spiral-out imaging and TE = 11.6 ms for the spiral-in case. Recognizing that the OSSI acquisition has some inherent T_2^*-weighting with spiral-out effective TE = 17.5 ms and spiral-in effective TE = 27.5 ms according to the simulations, we used slightly varying GRE TEs for different experiments to get an robust real data estimation of OSSI effective TE. For the 4 spiral-out experiments, we selected GRE TE = 17.5, 20, 20, and 23 ms, and for the 4 spiral-in experiments, we selected GRE TE = 27.5, 30, 30, and 33 ms.

Additionally, a T_1-weighted image was acquired for each subject and used to create a mask for the brain regions using the Brain Extraction Tool [17].

3.2.2 | 3D Human Studies

As an anecdotal demonstration, we acquired a 3D data set for a single human subject. The functional study was the same visual stimulus as in 2D studies (5 cycles of 20s on/20s off). An oblique 12-slice 3D volume was acquired using a stack of single-shot spirals with spiral-out readouts. The matrix size = $64 \times 64 \times 12$, and the voxel size = $3.44 \times 3.44 \times 3$ mm^3. For 3D OSSI imaging, TR = 15 ms, n_c = 10, FA = 10°, TE = 2.2 ms for each slice, and the volume TR = 1.8 s (TR$\cdot$ n_c $\cdot$ n_z). The spiral sampling trajectory in the k_x-k_y plane was a variable-density spiral with a linearly decreasing sampling density, leading to a factor of 3 undersampling. Along the k_z direction, the spirals were rotated 45° for each spiral platter to reduce undersampling artifacts. For the GRE imaging, the 12 slices were collected using a 2D spiral-out sequence with fully sampled uniform-density spirals, GRE TR = 1.8 s, TE = 23 ms to approximately match OSSI effective TE, and FA = 75°. The number of volumes = 112 for both OSSI (after 2-norm combination) and GRE, for a total about 200 s of acquisition, which followed 10 s of

discarded acquisition used to establish the steady state.

We also acquired 2D multi-slice images using a standard spin-warp acquisition for generating SENSE maps. The 32-channel coil images were compressed to 28 virtual coils, and the SENSE maps were generated using ESPIRiT [18, 19]. The 3D OSSI images were reconstructed from the undersampled measurements using the conjugate gradient SENSE [20, 21], with an edge-preserving regularizer implemented through [22]. The fully sampled GRE data were reconstructed using the gridding method.

3.3 | Data Analysis

As mentioned above, every n_c = 10 consecutive and non-overlapping OSSI images were combined by taking the 2-norm. Functional imaging performance was evaluated for both OSSI and GRE BOLD by evaluating activation maps and the temporal SNR (tSNR). The data from the first cycle (40 s) of the task were discarded to avoid the modeling error in the initial rest period. To reduce the effects of scanner drift, detrending was applied using lower order discrete cosine transform bases. The correlation coefficients were determined by correlation with a reference waveform, and the activated regions were defined by the magnitude of the correlation coefficients larger than a 0.5 threshold. The reference waveform was generated by convolving the canonical hemodynamic response function [23] with the task. The number of activated voxels were counted at the bottom third of the brain, where the primary visual cortex is located. The tSNR maps were calculated by dividing the mean of the time course by the standard deviation of the time course residual (after removing the mean and the task) for each voxel. We calculated the average tSNR over the whole brain over an ROI limited to the brain region and excluding the skull and scalp.

To determine the effective TE of OSSI, we generated scatter plots based on the percent signal change for voxels that were active in both GRE and OSSI acquisitions. In GRE, the percent signal change is approximately equal to $\Delta R_2' \cdot \mathrm{TE}$ [24]. By establishing the relationship between OSSI and GRE percent change and under the assumption that activation change ($\Delta R_2'$) is the same in both cases, we can estimate the effective TE for OSSI using $\mathrm{TE}_{\mathrm{eff}} = b \cdot \mathrm{TE}_{\mathrm{GRE}}$ when the percent changes of OSSI and GRE are highly correlated, where b is the slope of the OSSI-GRE percent change relationship. Due to variability in both data sets, we performed a model II fit with standardized major axis (SMA) regression and 0 intercept to estimate the slope of the relationship for each experiment. Voxels with a percent change greater than 4% in either method, which likely represent vascular signals, were found to be highly variable and were excluded from the regression. In addition, the linearity of the relationship between OSSI and GRE percent signal changes was assessed using Pearson's correlation coefficient.

4 | RESULTS

The phantom images in Figure 4 (a) present the evolution of the oscillation pattern for OSSI over the n_c = 10 phase cycles and show the highly reproducible nature of the oscillations. Note that magnetic field inhomogeneity leads to an inhomogeneous spatial pattern in the

OSSI data, and that different isochromats have different temporal patterns. Figure 4 (b) shows the same slice with spoiled gradients. Although the spoiled steady-state images are free of oscillations, their magnitudes are much lower. The 2-norm combination of every non-overlapping n_c = 10 OSSI images produces spatially and temporally uniform signals. The time courses in Figure 5 show oscillating steady-state signal and the stable signal after the 2-norm combination. In comparison to spoiled GRE with matched resolutions and TE, the OSSI signal strength was roughly 2 times larger than the spoiled signal, though the exact relationship is highly dependent on phantom/tissue T_1s and T_2s.

Figure 6 gives 2D human spiral-out activation maps, time courses, and tSNR maps for visual stimulation. Compared to GRE with matched acquisition characteristics and TE, the OSSI result shows more activations according to the activation maps, a larger task-related signal change as in the time course, and higher tSNR presented by the tSNR maps. The OSSI signals appear localized more in parenchyma with less signal from the sulci and vascular regions near the sagittal sinus.

Figure 7 shows 2D human spiral-in functional results and tSNR maps. The OSSI acquisition results in larger activation regions and much higher tSNR in comparison to GRE. Though anecdotal, the time course of OSSI appears to be less noisy. The spiral-in scheme uses a closer to optimal TE for fMRI (at 3T, a common choice is TE = 30 ms), thereby leading to more activations for both OSSI and GRE compared to the spiral-out results in Figure 6 in spite of the overall lower signal intensity and tSNR.

Figure 8 shows OSSI and GRE percent signal change scatter plots for spiral-out data of Figure 6 and spiral-in data of Figure 7, and the slope of the scatter plots depicts the relationships between OSSI effective TE and GRE TE. The slope resulted from the SMA regression is 0.73 for spiral-out and 0.82 for spiral-in. As described in Methods, we can calculate the effective TE for OSSI as spiral-out OSSI TE_{eff} = 16.7 ms, and spiral-in OSSI TE_{eff} = 27.1 ms for this subject. Scatter plots for the other subjects can be found in the Supporting Information, Figure S7. The mean OSSI TE effective across all the subjects is 17.8 ms for spiral-out, and is 27.1 ms for spiral-in, given the actual TE's of 2.7 ms and 11.6 ms, respectively, which correspond to an effective T_2'-weighting of about 15 ms at the time of the excitation pulse for both spiral-out and spiral-in cases. The average correlation coefficient between OSSI and GRE across all subjects was 0.5, and linearity of the relationship was found to be significant ($p < 0.05$) for all data sets. The high correlation of OSSI and GRE percent signals in the common activated regions is consistent with a similar contrast mechanism for OSSI and GRE acquisitions.

Quantitative measurements for all visual fMRI experiments including number of activated voxels (at the bottom third of the brain) and average tSNR of the whole brain are given in Table 1. OSSI shows a 1.84 ratio (s.d. = 0.5) of number of activation voxels in comparison to GRE with matched spatial-temporal resolutions and similar effective TEs. The tSNR ratio of OSSI to GRE has a mean of 1.83 (s.d. = 0.19). tSNR values were compared using a paired t-test, and OSSI was found to be significantly higher ($p < 0.05$). The columns in Table 1 directly corresponds to the columns in Supporting Information Figure S4, which presents activation maps and tSNR maps for the 5 subjects. For each subject and GRE TE ranging from 17.5 ms to 33 ms, the OSSI acquisition provides larger activation regions and higher tSNR than GRE. Subject 2 demonstrated motion artifacts, which led to lower tSNR ratios, artifacts in

the tSNR maps, and some false positive activations (near the edge of the brain). The circular spatial variation in tSNR maps are believe to result from pulsatile flow at ventricles and vessels in combination with the multi-shot (8-shot) acquisition. When averaging tSNR over an ROI that is away from artifacts, the tSNR ratio of OSSI to GRE is generally greater than 2.

Figure 9 is a preliminary demonstration of 3D activation results in visual cortex. OSSI and GRE acquisitions give comparable activation maps even through the OSSI data were undersampled. For OSSI, the number of activated voxels = 705 and the average tSNR = 57.2. For GRE, the number of activated voxels = 883 and the average tSNR = 62.4.

5 | DISCUSSION

This paper describes a fundamentally new approach to fMRI acquisition that uses a novel oscillating steady-state source of signal that is very large and also sensitive to the blood oxygenation, thereby offering the potential for high SNR fMRI. The proposed quadratic phase progression in conjunction with balanced gradients produces this new steady state. As with other steady-state imaging methods, the OSSI method has large signals because it reuses rather than spoils the magnetization. The oscillating steady-state signals available prior to gradient dephasing contain typically more than twice the average signal amplitude of spoiled signals. We have also noted that this pulse sequence with its quadratic phase sequence is very sensitive to off-resonance. Indeed, a frequency dependent phase dispersal is important for generating the T_2'- or T_2^*-contrast that makes it suitable for fMRI. In our experiments, we found T_2'-weighting of approximately 15 ms at the time of excitation pulse. Additional T_2' weighting can be obtained with increased TE as shown in Supporting Information Figure S3.

OSSI signals oscillate with a periodicity of n_cTR, however, the oscillations are highly reproducible, and by combining n_c time points generates stable time courses required for fMRI analysis. As demonstrated in the high-resolution visual stimulation fMRI study, the OSSI approach improves tSNR by about 83% and the number of activated voxels was increased by about 84%, both relative to GRE imaging at the Ernst angle with the carefully matched spatial-temporal acquisition characteristics and effective TEs. The 2D human fMRI experiments used relatively high spatial resolution and thus were closer to thermal noise limit. The same data were subjected to low spatial resolution reconstructions with the results shown in the Supporting Information, Figure S10 and Table S1. While the OSSI data still had SNR advantages, the SNR gain of OSSI was reduced relative to the high-resolution and more thermal noise limited cases. Similarly for the anecdotal low-resolution 3D human data that was likely to be physiological noise limited and for the low-resolution phantom data that is systematical noise limited [25], the SNR advantage is compromised.

Because we acquired GRE with a longer TE, there is a possible concern that the longer TR might alter temporal noise characterstics, so we compared the OSSI method to GRE with a 3× shorter GRE TR. As shown in Supporting Information Figure S11 and Table S2, for the experimental conditions used (high spatial resolution, likely thermal noise limited regime), the shorter TR leads to similar functional results and tSNR values as GRE with longer TR. We also considered the possible use of other steady state methods, such as FISP/S1 SSFP and found that while it has more signal than GRE for short TRs, it does not have the increased T_2^*

sensitivity of OSSI.

We note that further improvements in performance are possible and in fact, likely. For example, our simulations show that TR = 15 ms, n_c = 10, and FA = 10° is a good combination to get high SNR and functional MRI responses, but it is by no means optimal. The short readouts can limit SNR efficiency, so there are potential advantages to going to longer TRs and longer readouts. As shown in Figure 3 and Supporting Information Figure S1, multiple combinations of imaging parameters give a similar T_2^*-sensitivity and off-resonance sensitivity. There is a complex interplay between these sensitivity measures and the major imaging parameters including TR, n_c, FA, and TE (including TE locations from different readouts, e.g. spiral-out, spiral-in, or EPI with TE in the center). The RF (FA) inhomogeneity in the brain at 3T may influence the actual FA to use when acquiring slices at different parts of the brain, which further complicates the optimization. We also note that the optimal FA appears to be small in comparison to many bSSFP applicaitons where FAs $> 30°$ are common, which would indicate that RF heating is unlikely to be an issue with OSSI. Curiously, the optimal FAs are often not far from the Ernst angle, e.g. 8.3° for TR = 15 ms. The final optimization will require practical experience regarding which factors are most important for particular fMRI studies.

The sensitivity to frequency as noted above, will lead to substantial physiological noise, and in particular, artifacts and noise from respiration, which is known to lead to oscillations shifts in resonant frequency [26]. Figure S9 presents residual time courses and spectra of OSSI and GRE at a non-active region, and the OSSI spectrum shows a prominent peak near respiration frequencies. We investigated the standard physiological noise removal technique RETROICOR [27] applied to individual temporal phases as well as the combined images, and also k-domain methods (RETROKCOR [28]) applied to individual temporal phases. We found only modest improvements in tSNR and activation maps when applying corrections over limited time windows and no improvements over longer windows [29]. This, we believe, is due to the complex and non-linear nature of the interaction between frequency and the temporal signal (see Figure 2 (c, d), for example). In addition, the use of a 2D slice for the visual study makes it sensitive to inflow and pulsatility artifacts. Physiological noise correction is an active area of research [30] and will be the topic of a future manuscript. As such, no physiological noise corrections for OSSI were applied in the present work, but we believe that after correction, further tSNR and activation improvements close to the increases in signal strength will be possible.

Like most steady-state methods, the short TR largely prevents interleaving of slices, when combined with the time needed to reach steady state, dictates that OSSI methods are best suited to 3D acquisitions. Furthermore, the need to acquire volumetric images for each temporal phase implies that n_c times as many images are required for a study. Fortunately, the reproducible nature of oscillating signal may allow dramatic reductions in the acquisition time. For example, the use of sparse sampling in k-space and modeling of the oscillations using patch-tensor low-rank [31] or a dictionary based regularizer [32] can fully recover the missing data in the image reconstruction process. This again, is a topic of active research, and preliminary results suggest that larger than a 13-fold reduction in k-space is possible with minimal performance degradation. We have anecdotally demonstrated the ability to acquire 3D images, though without acceleration using the spatiotemporal models described here. We

note that most 2D acquisitions would include acceleration using 2D simultaneous multi-slice imaging [33, 34], but also note that undersampling in 3D exploits roughly the same parallel imaging concepts [35]. So, we believe that similiar accelerations are possible for OSSI and the use of temporal modeling will help resolve the inefficiency of acquiring n_c images. The slow volume TR reduces temporal resolution, but does not reduce SNR due to averaging of signal and noise across the n_c temporal phases. As pointed out above, the short TR does limit the length of the readout which can reduce the SNR efficiency.

In prior work, bSSFP imaging for fMRI has taken advantage of different phenomena, for example, frequency shifts, changes in T_2 associated with changes in blood oxygenation, or changes due to inhomogeneous effects and diffusion around small vessels [6, 7]. In this work, we argue that the OSSI signal changes are due to more traditional, size-scale invariant changes in T_2^* or T_2' of the tissues, again in response to changes in blood oxygenation. We argue that this sensitivity is due to frequency sensitivity of OSSI signal that leads to frequency-dependent phase variations as shown in the simulations of Figure 1 (d). The percent signal plots in Figure 8 and Figure S7 clearly show a very linear relationship (average p-value for the slope = 0.01 using standard linear regression) of OSSI and GRE percent signal changes, which would be consistent with a similar signal change mechanism between the two methods. We note that further work is necessary to fully elucidate the mechanism, including the effects of diffusion around vessels. The simulation and percent signal change analysis are both consistent with the OSSI signal being inherently T_2^* or T_2' weighted, specifically OSSI leads to an additional T_2'-weighting of approximately 15 ms for the parameters used (TR = 15 ms, n_c = 10, FA = 10°).

The analysis of percent change signal in OSSI and GRE excluded voxels with a percent change greater than 4% in at least one of the methods. Above 4%, the signal change for OSSI seemed to flatten and the relationship was no-longer suitable for linear regression. These very high GRE percent changes, which likely represent vascular signals as shown in Figure S8, have had a lower signal change in OSSI perhaps due to flow-related signal changes. If so, this partial suppression of vascular signals could be seen as a desirable feature as it will improve functional localization.

There are a number of unstudied phenomena we wish to address in the future. Long T_2-species like cerebrospinal fluid in the ventricles are very bright in OSSI, but when combined with cardiac pulsatility lead to low tSNR as seen in the first and third rows of Figure S4. Part of the high variability may arise from the in-flow effects associated with the 2D acquisition and may be partially resolved by 3D imaging. Pulsatile effects and in-flow phenomena with vessels require further investigation. The short TR makes implementation of fat suppression more challenging, however, the relaxation and spectral characteristics of lipids seem to lead to relatively low signal intensity and limited artifacts in the images. Still, the signal characteristics of lipids, as well as the possible use of slab-selective spectral spatial pulses, should be investigated. As with most fMRI studies, detection and bulk correction of head motion will be needed. In this case, we will also need to consider any impact on the steady-state signal due to head motion.

Another interesting question is what occurs in the presence of large magnetic fields gradients near regions of large susceptibility differences in the brain, for example, the orbitofrontal

cortex. Such gradients might have a similar impact as applying unbalanced gradients, leading to signal spoiling and a reduction of the additional T_2'-weighting of 15 ms common to OSSI. The signal may gracefully transition to a spoiled GRE signal with relatively short TE. This phenomenon is closely related to partial spoiling described by Ganter [36], except that very small phase increments with large gradients are used in Ganter's paper, while here we have large phase increments between RF pulses but partial gradient spoiling. We are also interested in other possible applications of the OSSI signal. Frequency sensitivity may be useful in applications where frequency tracking is needed, for example, in tracking temperature-dependent frequency changes in therapeutic ultrasound.

6 | CONCLUSION

The OSSI approach departs from traditional acquisition approaches by exploiting a novel T_2^*-weighted signal mechanism that produces large steady-state signals, and to our knowledge, has never been used before for fMRI. We show in both simulations and experimental data that the proposed approach has a similar contrast mechanism and percent signal change as GRE and leads to a substantial increase in signal strength and tSNR with matched spatial-temporal resolutions and effective TE, thereby enabling detection of 84% greater volumes of functional activity. The SNR advantages were shown for a specific case of single slice fMRI using a short TR, and extensions to volumetric acquisition and implementation of physiological noise corrections will be critical for general application. Still, this approach offers the prospect of high-resolution fMRI without the need for higher magnetic field strength systems.

Acknowledgements

The authors acknowledge important discussions and assistance of Amos Cao, Tianrui Luo, Dr. Scott Peltier, and Dr. Jeffrey Fessler.

references

[1] van Gelderen P, Ramsey NF, Liu G, Duyn JH, Frank JA, Weinberger DR, et al. Three-dimensional functional magnetic resonance imaging of human brain on a clinical 1.5-T scanner. Proceedings of the National Academy of Sciences of the United States of America 1995 jul;92(15):6906–10.

[2] Rettenmeier C, Maziero D, Qian Y, Stenger VA. A circular echo planar sequence for fast volumetric fMRI. Magnetic Resonance in Medicine 2019 mar;81(3):1685–1698.

[3] Sun H, Fessler JA, Noll DC, Nielsen JF. Steady-state functional MRI using spoiled small-tip fast recovery imaging. Magnetic Resonance in Medicine 2015 feb;73(2):536–543.

[4] Scheffler K, Seifritz E, Bilecen D, Venkatesan R, Hennig J, Deimling M, et al. Detection of BOLD changes by means of a frequency-sensitive trueFISP technique: preliminary results. NMR in Biomedicine 2001 nov;14(7-8):490–496.

[5] Miller KL, Hargreaves BA, Lee J, Ress D, Christopher deCharms R, Pauly JM. Functional brain imaging using a blood oxygenation sensitive steady state. Magnetic Resonance in Medicine 2003 oct;50(4):675–683.

[6] Zhong K, Leupold J, Hennig J, Speck O. Systematic investigation of balanced steady-state free precession for functional MRI in the human visual cortex at 3 Tesla. Magnetic Resonance in Medicine 2007 jan;57(1):67–73.

[7] Miller KL, Jezzard P. Modeling SSFP functional MRI contrast in the brain. Magnetic Resonance in Medicine 2008 sep;60(3):661–673.

[8] Scheffler K, Ehses P. High-resolution mapping of neuronal activation with balanced SSFP at 9.4 tesla. Magnetic Resonance in Medicine 2016 jul;76(1):163–171.

[9] Scheffler K, Maderwald S, Ladd ME, Bieri O. Oscillating steady states. Magnetic Resonance in Medicine 2006 mar;55(3):598–603.

[10] Overall WR, Conolly SM, Nishimura DG, Hu BS. Oscillating dual-equilibrium steady-state angiography. Magnetic Resonance in Medicine 2002 mar;47(3):513–522.

[11] Zur Y, Wood ML, Neuringer LJ. Spoiling of transverse magnetization in steady-state sequences. Magnetic Resonance in Medicine 1991 oct;21(2):251–263.

[12] Foxall DL. Frequency-modulated steady-state free precession imaging. Magnetic Resonance in Medicine 2002 sep;48(3):502–508.

[13] Wang CY, Coppo S, Mehta BB, Seiberlich N, Yu X, Griswold MA. Magnetic resonance fingerprinting with quadratic RF phase for measurement of T_{2*} simultaneously with δ_f, T_1, and T_2. Magnetic Resonance in Medicine 2019 mar;81(3):1849–1862.

[14] Relaxation Times;. https://itis.swiss/virtual-population/tissue-properties/database/relaxatio

[15] Boxerman JL, Hamberg LM, Rosen BR, Weisskoff RM. Mr contrast due to intravascular magnetic susceptibility perturbations. Magnetic Resonance in Medicine 1995 oct;34(4):555–566.

[16] Glover GH, Mueller BA, Turner JA, van Erp TGM, Liu TT, Greve DN, et al. Function biomedical informatics research network recommendations for prospective multicenter functional MRI studies. Journal of magnetic resonance imaging : JMRI 2012 jul;36(1):39–54.

[17] Smith SM. Fast robust automated brain extraction. Human Brain Mapping 2002 nov;17(3):143–155.

[18] Uecker M, Lai P, Murphy MJ, Virtue P, Elad M, Pauly JM, et al. ESPIRiT–an eigenvalue approach to autocalibrating parallel MRI: where SENSE meets GRAPPA. Magnetic resonance in medicine 2014 mar;71(3):990–1001.

[19] BART Toolbox for Computational Magnetic Resonance Imaging;. https://mrirecon.github.io/bart/.

[20] Pruessmann KP, Weiger M, Börnert P, Boesiger P. Advances in sensitivity encoding with arbitrary k-space trajectories. Magnetic resonance in medicine 2001 oct;46(4):638–51.

[21] Sutton BP, Noll DC, Fessler JA. Fast, iterative image reconstruction for MRI in the presence of field inhomogeneities. IEEE Transactions on Medical Imaging 2003 feb;22(2):178–188.

[22] Michigan Image Reconstruction Toolbox;. https://web.eecs.umich.edu/~fessler/code/index.html.

[23] Statistical Parametric Mapping;. https://www.fil.ion.ucl.ac.uk/spm/.

[24] Jin T, Wang P, Tasker M, Zhao F, Kim SG. Source of nonlinearity in echo-time-dependent BOLD fMRI. Magnetic Resonance in Medicine 2006 jun;55(6):1281–1290.

[25] Krüger G, Glover GH. Physiological noise in oxygenation-sensitive magnetic resonance imaging. Magnetic Resonance in Medicine 2001;46(4):631–637.

[26] Noll DC, Schneider W. Theory, simulation, and compensation of physiological motion artifacts in functional MRI. In: Proceedings of 1st International Conference on Image Processing, vol. 3 IEEE Comput. Soc. Press;. p. 40–44.

[27] Glover GH, Li TQ, Ress D. Image-based method for retrospective correction of physiological motion effects in fMRI: RETROICOR. Magnetic resonance in medicine 2000 jul;44(1):162–7.

[28] Hu X, Le TH, Parrish T, Erhard P. Retrospective estimation and correction of physiological fluctuation in functional MRI. Magnetic resonance in medicine 1995 aug;34(2):201–12.

[29] Guo S, Noll DC. High SNR Functional MRI Using Oscillating Steady State Imaging. In: Proceedings of International Society for Magnetic Resonance in Medicine, Paris; 2018. p. 5441.

[30] Cao AA, Guo S, Noll DC. Dynamic model-based reconstruction for oscillating steady state fMRI. In: Proceedings of the 27th Annual Meeting of ISMRM, Montreal; 2019. p. 3771.

[31] Guo S, Noll DC. Patch-tensor low-n-rank reconstruction for oscillating steady state fMRI acceleration. In: Proceedings of the 26th Annual Meeting of ISMRM, Paris; 2018. p. 3531.

[32] Guo S, Noll DC, Fessler JA. Dictionary-based oscillating steady state fMRI reconstruction. In: Proceedings of the 27th Annual Meeting of ISMRM, Montreal; 2019. p. 1253.

[33] Moeller S, Yacoub E, Olman CA, Auerbach E, Strupp J, Harel N, et al. Multiband multislice GE-EPI at 7 tesla, with 16-fold acceleration using partial parallel imaging with application to high spatial and temporal whole-brain fMRI. Magnetic resonance in medicine 2010 may;63(5):1144–53.

[34] Setsompop K, Gagoski BA, Polimeni JR, Witzel T, Wedeen VJ, Wald LL. Blipped-controlled aliasing in parallel imaging for simultaneous multislice echo planar imaging with reduced g-factor penalty. Magnetic Resonance in Medicine 2012 may;67(5):1210–1224.

[35] Zahneisen B, Poser BA, Ernst T, Stenger VA. Three-dimensional Fourier encoding of simultaneously excited slices: generalized acquisition and reconstruction framework. Magnetic resonance in medicine 2014 jun;71(6):2071–81.

[36] Ganter C. Steady state of gradient echo sequences with radiofrequency phase cycling: Analytical solution, contrast enhancement with partial spoiling. Magnetic Resonance in Medicine 2006 jan;55(1):98–107.

Supporting Information

FIGURE S1

Simulation of acquisition parameters for spiral-in readouts (TE = TR - 1.6 ms). (a) to (c) are in units of M_0 = 1.

(a) shows the RMS combined magnitude signal as a function of n_c and flip angle for a fixed TR of 15 ms. We focus on the region denoted by the blue square for OSSI fMRI acquisition parameter optimization, and the results are given in (b) to (e). (b) shows how T_2^* sensitivity ($S_{activated} - S_{rest}$) varies with TR and flip angle for a fixed n_c = 10. The signal is normalized by $\sqrt{(TR - c)/TR} \approx \sqrt{T_{A/D}}$ with c = 5 ms for SNR efficiency. (c) shows how T_2^* sensitivity varies with n_c and flip angle for TR = 15 ms. (d) gives off-resonance sensitivity at different TR and flip angles for n_c = 10. (e) gives off-resonance sensitivity at different n_c and flip angles for TR = 15 ms.

FIGURE S2

T_2^*-sensitivity ($S_{activated} - S_{rest}$ in units of M_0) changes with varying TR for GRE spiral-in (TE = TR - 1.6 ms), OSSI spiral-out (TE = 1.6 ms), and OSSI spiral-in (TE = TR - 1.6 ms). The signals are normalized by $\sqrt{(TR - c)/TR} \approx \sqrt{T_{A/D}}$ with c = 5 ms for SNR efficiency and are maximized over flip angle for each method.

FIGURE S3

Simulated OSSI T_2^*-weighting and percent signal increase almost linearly with increased TE for TR = 15 ms, n_c = 10, and flip angle = 10°.

FIGURE S4

Comparison of OSSI and GRE activation maps and tSNR maps for all 5 subjects.

FIGURE S5

Z-maps of all the experiments.

FIGURE S6

Histograms of voxel counts over z-score threshold = ±7, which corresponds to correlation = ±0.5 for the GRE TR = 150 ms case.

FIGURE S7

Percent signal change of OSSI vs. GRE for active voxels for subjects 2-5 where the percentage signal change was below 4% in both methods. Actual OSSI TE is 2.7 ms for spiral-out and is 11.6 ms for spiral-in.

These figures demonstrate a high correlation between the methods, indicating the potential utility of OSSI as an alternative to GRE fMRI. The slope of the line was fit via Model II regression.

(a) subject 2 spiral-out acquisition, GRE TE = 20 ms, slope = 1.05, and OSSI TE_{eff} = 21 ms.
(b) subject 2 spiral-in acquisition, GRE TE = 30 ms, slope = 1.06, and OSSI TE_{eff} = 31.7 ms.
(c) subject 3 spiral-out acquisition, GRE TE = 17.5 ms, slope = 0.83, and OSSI TE_{eff} = 14.5 ms.
(d) subject 3 spiral-in acquisition, GRE TE = 27.5 ms, slope = 0.85, and OSSI TE_{eff} = 23.2 ms.
(e) subject 4 spiral-out acquisition, GRE TE = 20 ms, slope = 0.95, and OSSI TE_{eff} = 19 ms.
(f) subject 5 spiral-in acquisition, GRE TE = 30 ms, slope = 0.87, and OSSI TE_{eff} = 26.2 ms.

FIGURE S8

GRE background image with vasculature (left) and the activated voxels with > 4% percent signal changes overlaid to the GRE background image (right).

FIGURE S9

The residual time courses and spectra averaged over a larger ROI (20×20 voxels) away from the active regions after mean and drift removal. The large ROI eliminates the effect of thermal noise. The OSSI spectrum has higher physiological noise due, in part, to larger signals, but the presence of a prominent peak near respiration frequencies demonstrates potential greater sensitivity of physiological noise. The phyisological noise may cause the tSNR improvement to be less than that predicted from signal strength alone.

FIGURE S10

Comparison of OSSI and GRE activation maps and tSNR maps for all the experiments reconstructed at a lower spatial resolution.

FIGURE S11

Z-maps and tSNR maps of OSSI, GRE TR = 50 ms, and GRE TR = 150 ms for both spiral-out and spiral-in acquisitions. The z-score threshold = ±7 and corresponds to correlation = ±0.5 for the GRE TR = 150 ms case. For GRE TR = 50 ms, averaged images of every 3 time points are used for tSNR calculation.

TABLE S1

Quantitative results including number of activated voxels and average tSNR from low spatial resolution reconstructions.

TABLE S2

Quantitative measures including number of voxels beyond a z-score threshold of ±7 and average tSNR within the brain.

TABLE 1 Quantitative results including number of activated voxels and average tSNR.

		Spiral-Out				Spiral-In				
Subject ID		1	2	3	4	1	2	3	5	Mean (SD)
# Activated Voxels	OSSI	215	159	210	84	264	165	236	123	182
	GRE	133	113	116	55	151	84	144	41	105
	Ratio	1.62	1.41	1.81	1.53	1.75	1.96	1.64	3.0	1.84 (0.5)
Average tSNR	OSSI	85.1	55.1	74.7	68.2	71.4	47.2	60.6	47.9	63.8
	GRE	40.9	34.9	41.9	37.8	34.6	29.5	34.1	24.7	34.8
	Ratio	2.08	1.58	1.78	1.80	2.06	1.60	1.78	1.94	1.83 (0.19)

OSSI, oscillating steady-state imaging; GRE, gradient echo imaging; tSNR, temporal signal-to-noise ratio.

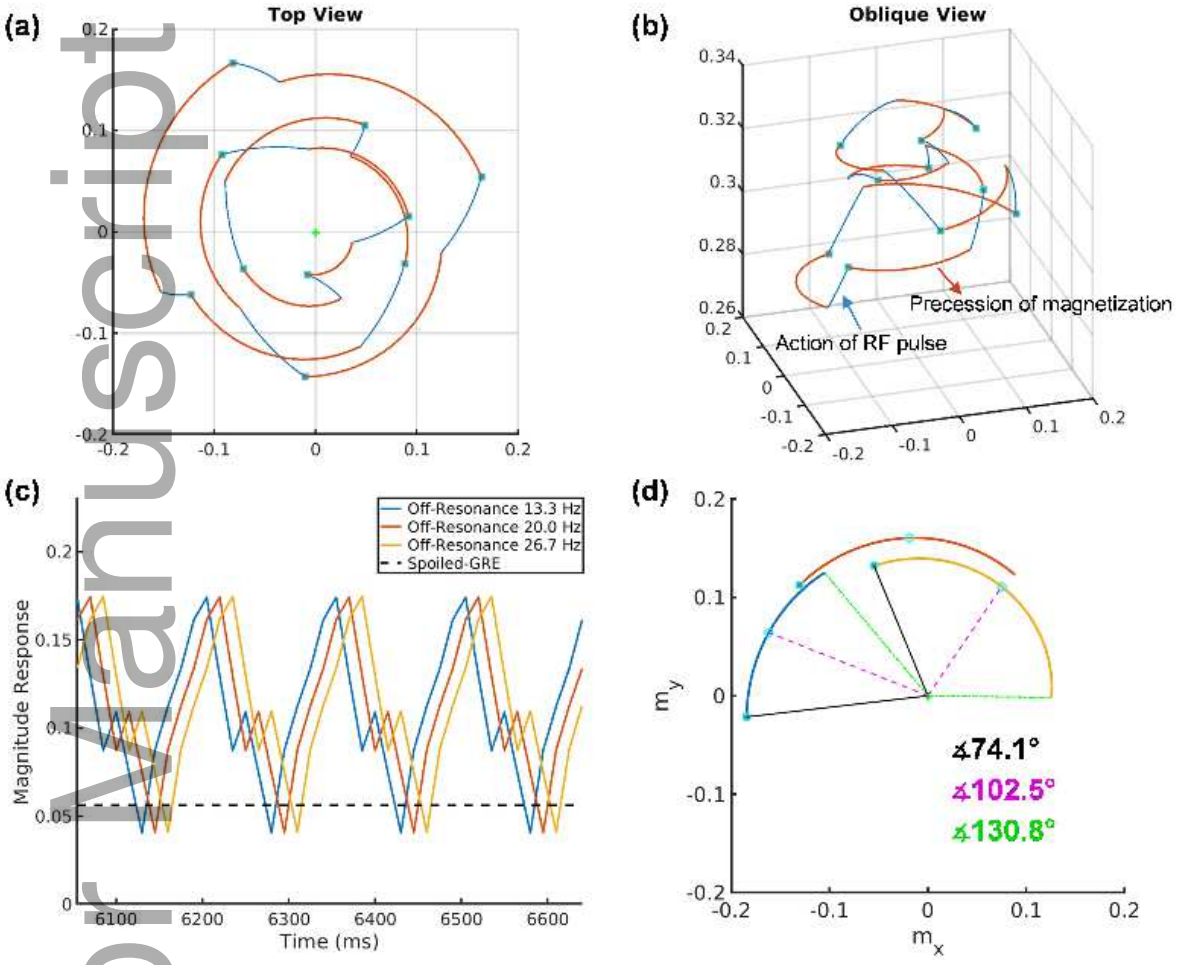

FIGURE 1 Simulation of OSSI spin behavior and signals.
(a) and (b) Periodic motion of magnetization through RF pulses (the filled squares are at the end of the RF pulse) and free precession for a gray matter spin at -20 Hz off-resonance frequency, T_1 = 1433.2 ms, T_2 = 92.6 ms, TR = 15 ms, n_c = 10, and FA = 10° from two different views. (c) Magnitude signal variation of different isochromats (6.67 Hz apart) for the magnetization in (a) and (b) just after the RF pulse, the black dashed line is the Ernst angle signal for spoiled-GRE. (d) Spin positions during free precession for different isochromats (same isocromats as in (c)) leading to phase dispersion and T_2^*-weighting. The cyan circles mark the center of the precession interval.

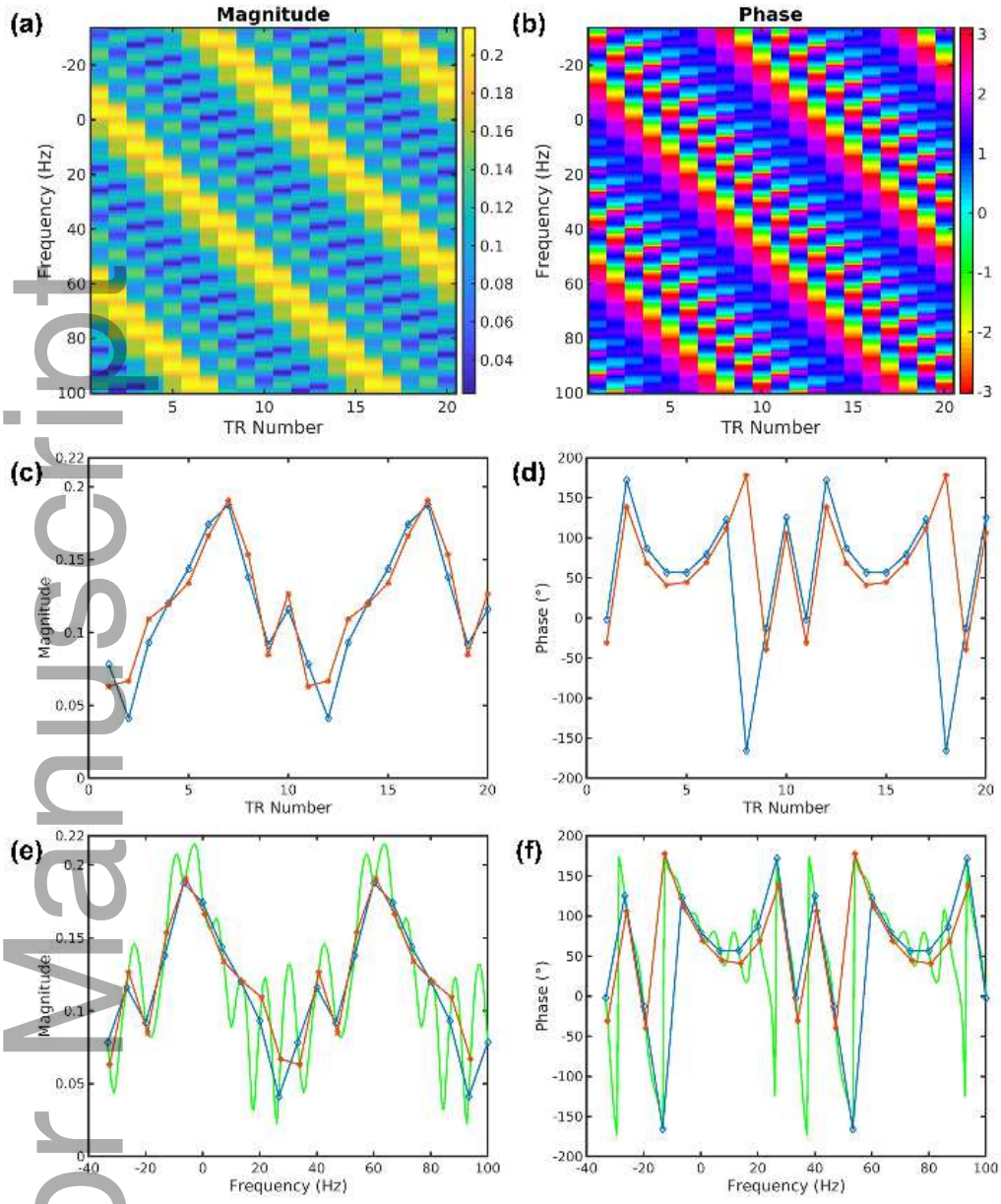

FIGURE 2 Simulation for signal properties just after the RF pulse, where the pulse duration was adjusted to minimize off-resonance phase accumulation during the RF pulses (TE < 0.02 ms). The left and right panels show simulated OSSI signal magnitude and phase, respectively. (a) and (b) show magnitude and phase responses as a function of off-resonance frequency and time (TR number), observe the periodicity in time ($T_{OSSI} = n_c TR$) and frequency (1/TR = 66.67 Hz). (c) and (e) are magnitude response of the signal vs. time and frequency, respectively, and (d) and (f) are the phase responses showing phases after correction for the excitation RF phase. The blue and red lines in temporal plots (c) and (d) correspond to two isochromats at off-resonance -33.33 Hz and -32.67 Hz, respectively. It can be seen that an off-resonance amount of less than $1/T_{OSSI}$ lead to some modest changes in the shape of the response. The green curve in (e) and (f) are the magnitude and phase of the frequency response, respectively, and indicate the manifold on which the steady-state response exists. The blue and red lines connect 6.67 Hz apart samples of the manifold and start from off-resonance -33.33 Hz and -32.67 Hz respectively. Particularly, by comparing (c) and (e), (d) and (f), it is clearly shown that the time and samples of frequency responses have exactly the same shape, only flipped.

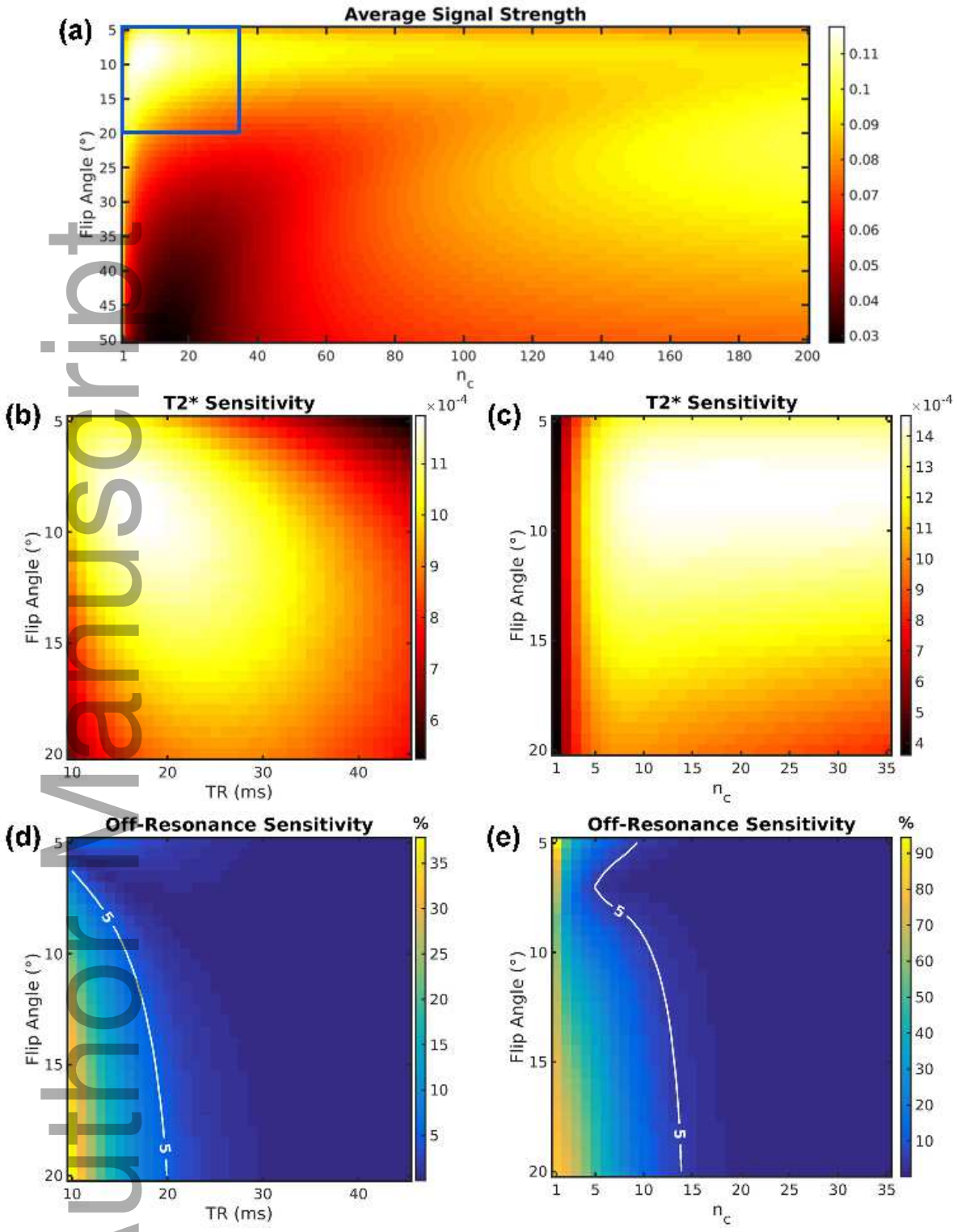

FIGURE 3 Simulation of acquisition parameters for spiral-out readouts (TE = 1.6 ms). (a) to (c) are T_2^* sensitivity defined as $S_{activated} - S_{rest}$ in units of $M_0 = 1$.
(a) shows the RMS combined magnitude signal as a function of n_c and flip angle for a fixed TR of 15 ms. Notice the bright spot around $n_c = 10$ and flip angle = 10°. We focus on the region denoted by the blue square for OSSI fMRI acquisition parameter optimization, and the results are in (b) to (e). (b) shows how T_2^* sensitivity varies with TR and flip angle for a fixed $n_c = 10$. The signal is normalized by $\sqrt{(TR - c)/TR} \approx \sqrt{T_{A/D}}$ with $c = 5$ ms for SNR efficiency. (c) shows how T_2^* sensitivity varies with n_c and flip angle for TR = 15 ms. (d) gives off-resonance sensitivity at different TR and flip angles for $n_c = 10$. (e) gives off-resonance sensitivity at different n_c and flip angles for TR = 15 ms.

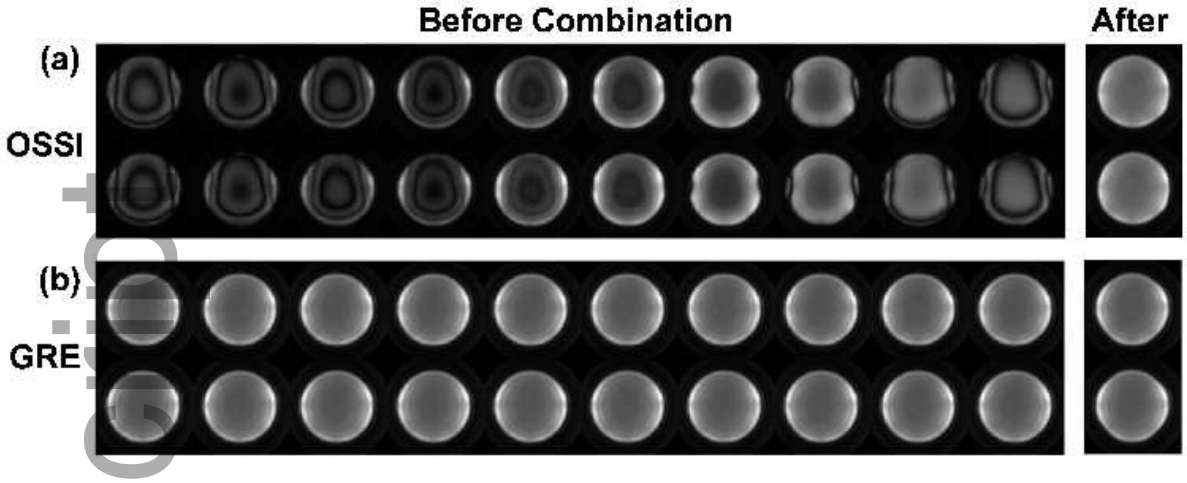

FIGURE 4 Images of steady state with quadratic phase progression (n_c = 10) with (a) balance gradients (OSSI) and (b) spoiling gradients (GRE). Each panel has 10 images across the periodic phase pattern and is shown twice to demonstrate the reproducibility. The 2-norm combined images are given on the right. The OSSI and GRE images are not on the same intensity scale.

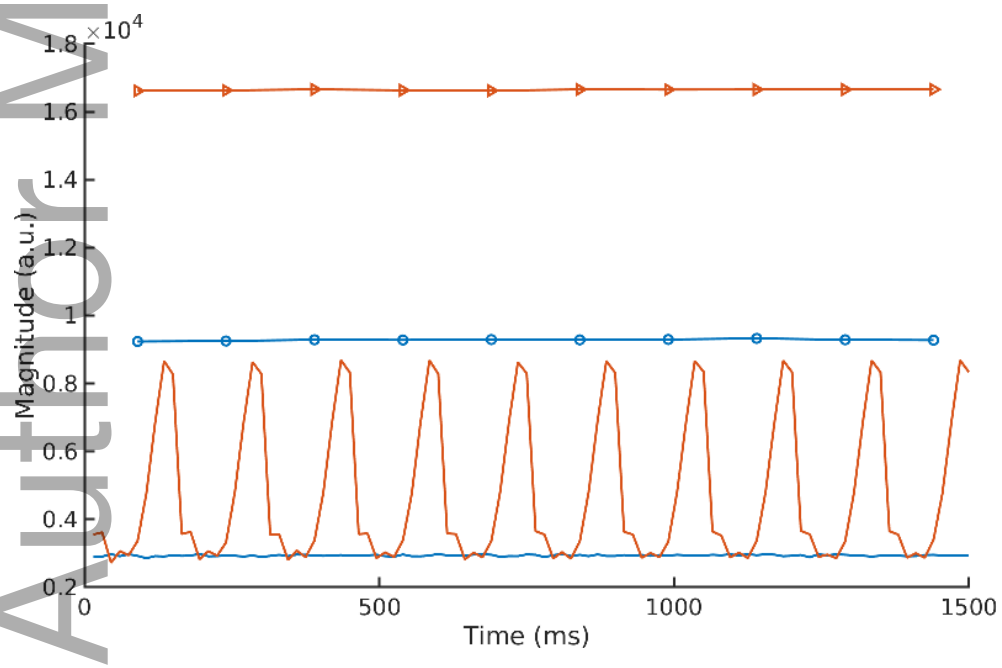

FIGURE 5 Time courses for a 4-voxel ROI in the phantom for OSSI (red) and GRE (blue). Both before and after 2-norm combination, OSSI shows signal strengths roughly two times larger than the spoiled GRE signal.

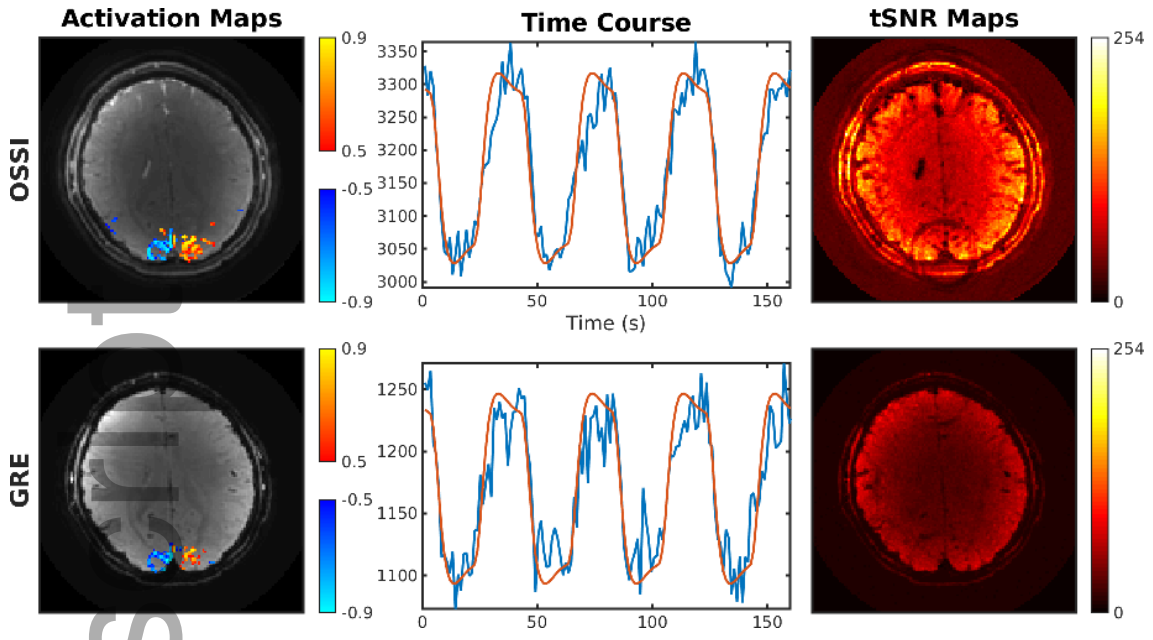

FIGURE 6 OSSI and GRE functional results from multi-shot spiral-out acquisition with OSSI TE = 2.7 ms and GRE TE = 23 ms. At left, the activation map uses a threshold of 0.5 for the correlation with a reference waveform, and the background is the mean image of the OSSI combined or GRE images. The time course for a 4-voxel ROI is shown for each method together with the reference waveform (intensity units are arbitrary signal units). At right, the temporal SNR maps are also shown for both methods.

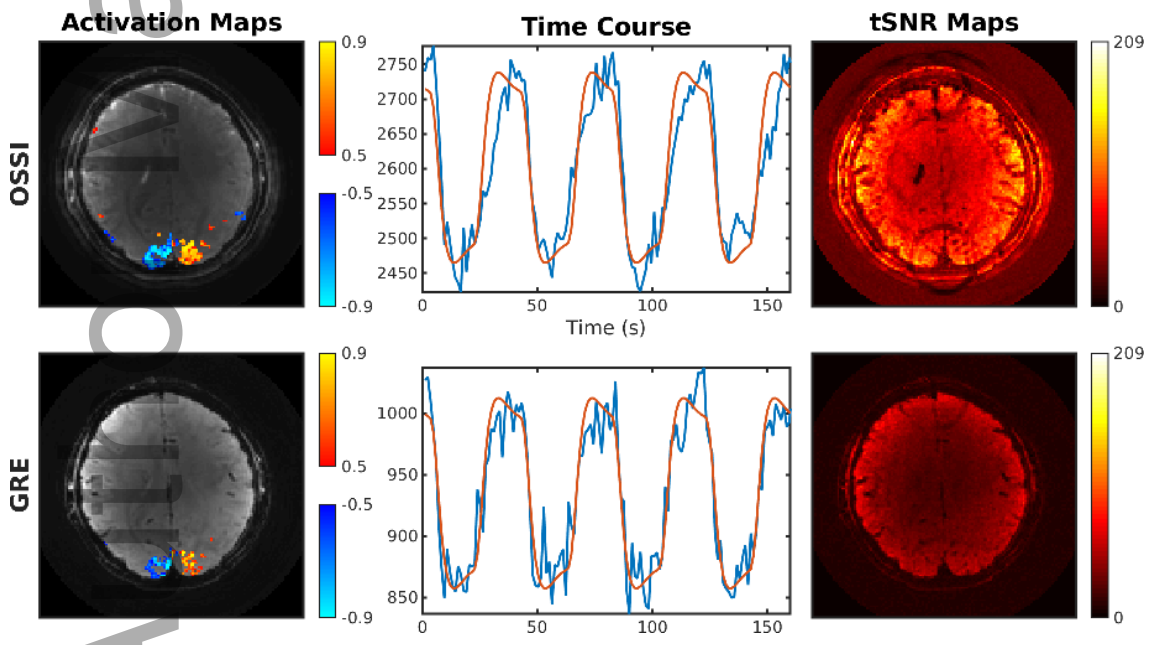

FIGURE 7 OSSI and GRE functional results from multi-shot spiral-in acquisition with OSSI TE = 11.6 ms and GRE TE = 33 ms. The activation map uses a threshold of 0.5 for the correlation with a reference waveform, and the time course for a 4-voxel ROI is shown with the reference waveform for each method (intensity units are arbitrary signal units). The temporal SNR maps are also shown for both OSSI and GRE acquisitions. Compared to the spiral-out results in Figure 6, we can see that spiral-in gives more activations, but relatively lower signal strength and temporal SNR for both OSSI and GRE.

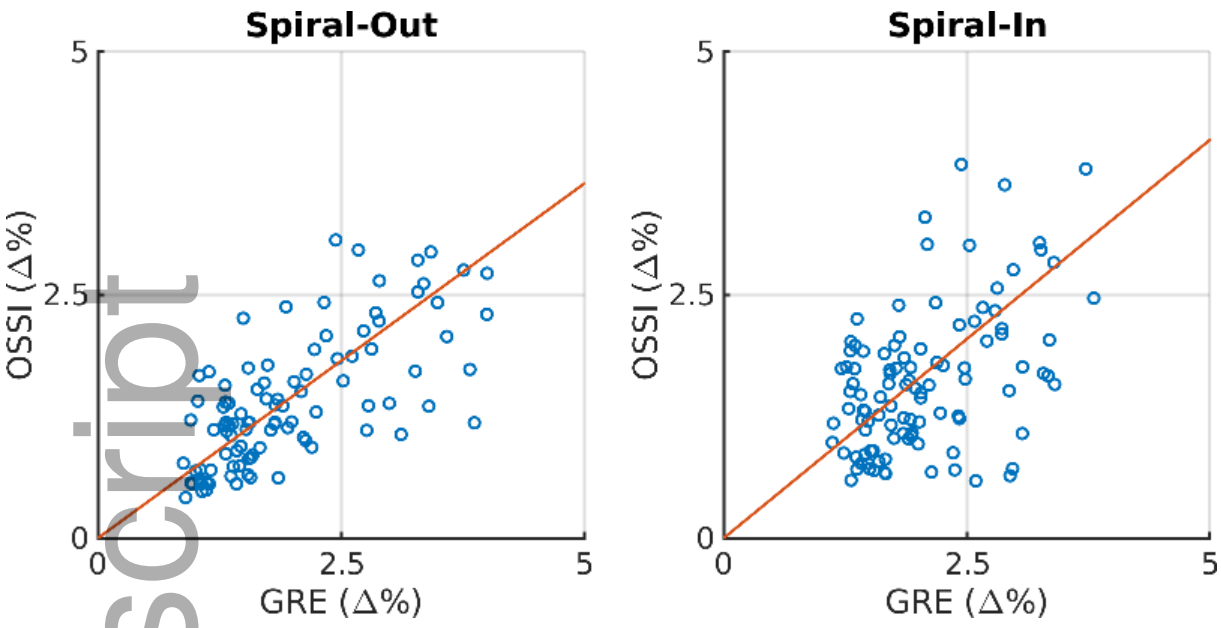

FIGURE 8 Percent signal change of OSSI vs. GRE for active voxels in Figure 6 and Figure 7 where the percentage signal change was below 4% in both methods (spiral out TEs: OSSI = 2.7 ms, GRE = 23 ms; spiral in: OSSI = 11.6 ms, GRE = 33 ms). These figures demonstrate a high correlation between the methods, indicating the potential utility of OSSI as an alternative to GRE fMRI. The slope of the line was fit via Model II regression.

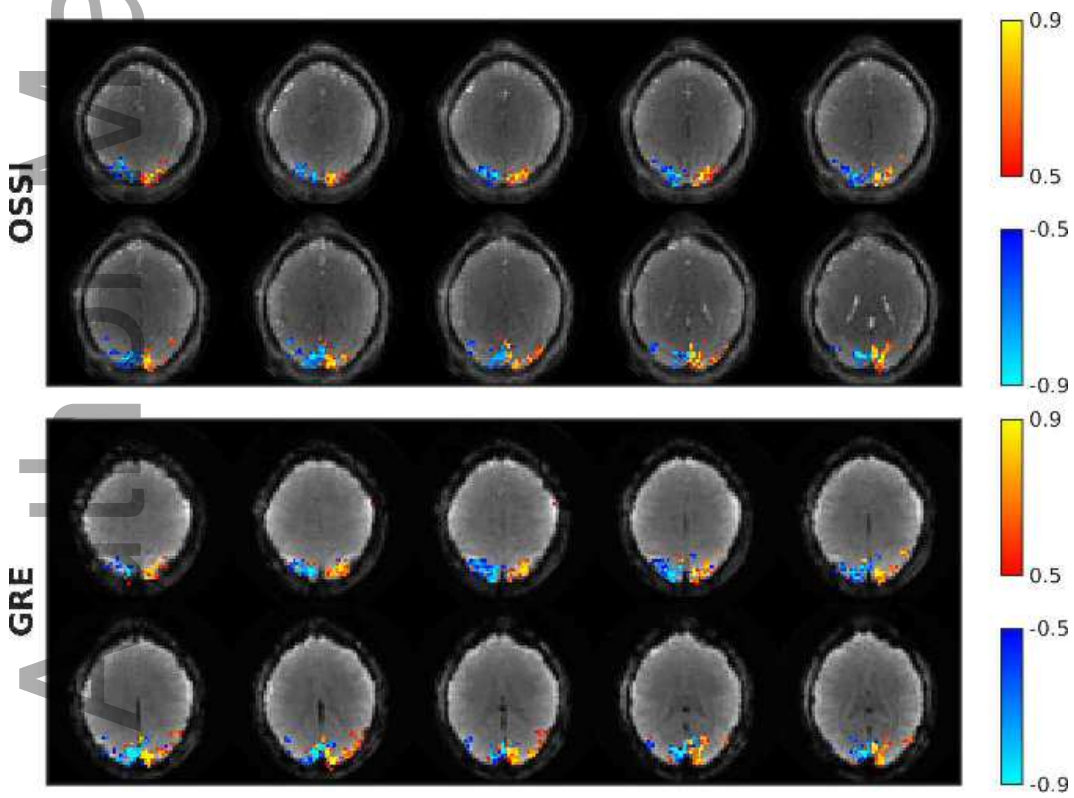

FIGURE 9 Functional MRI of 10 slices drawn from volumetric 3D OSSI acquisition (volume TR = 1.8 s, TE = 2.2 ms, matrix size = 64 through undersampling in-plane) and 2D multi-slice GRE (TR = 1.8 s, TE = 23 ms, matrix size = 64) showing similar activation patterns in visual cortex.

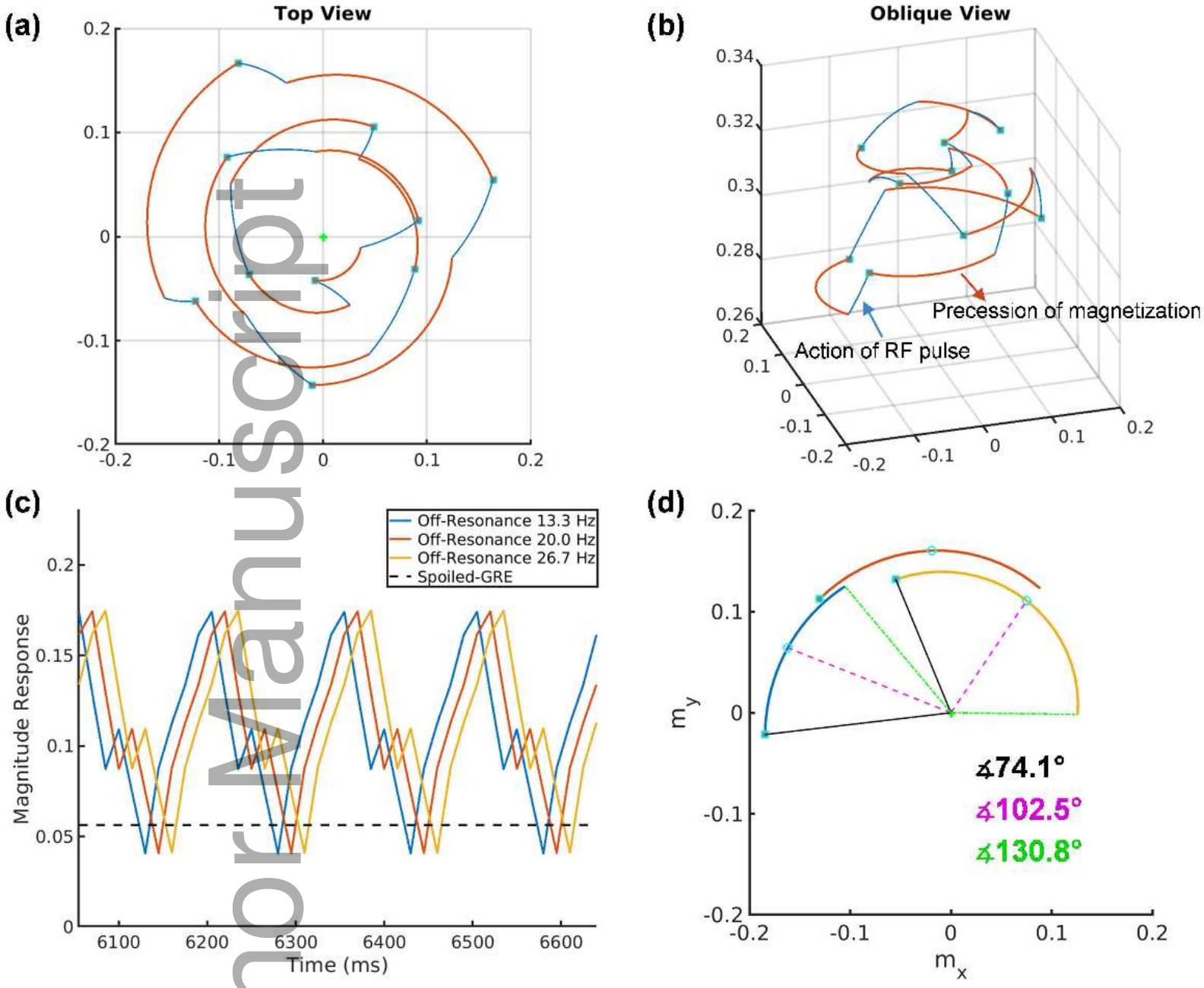

mrm_28156_f1.eps

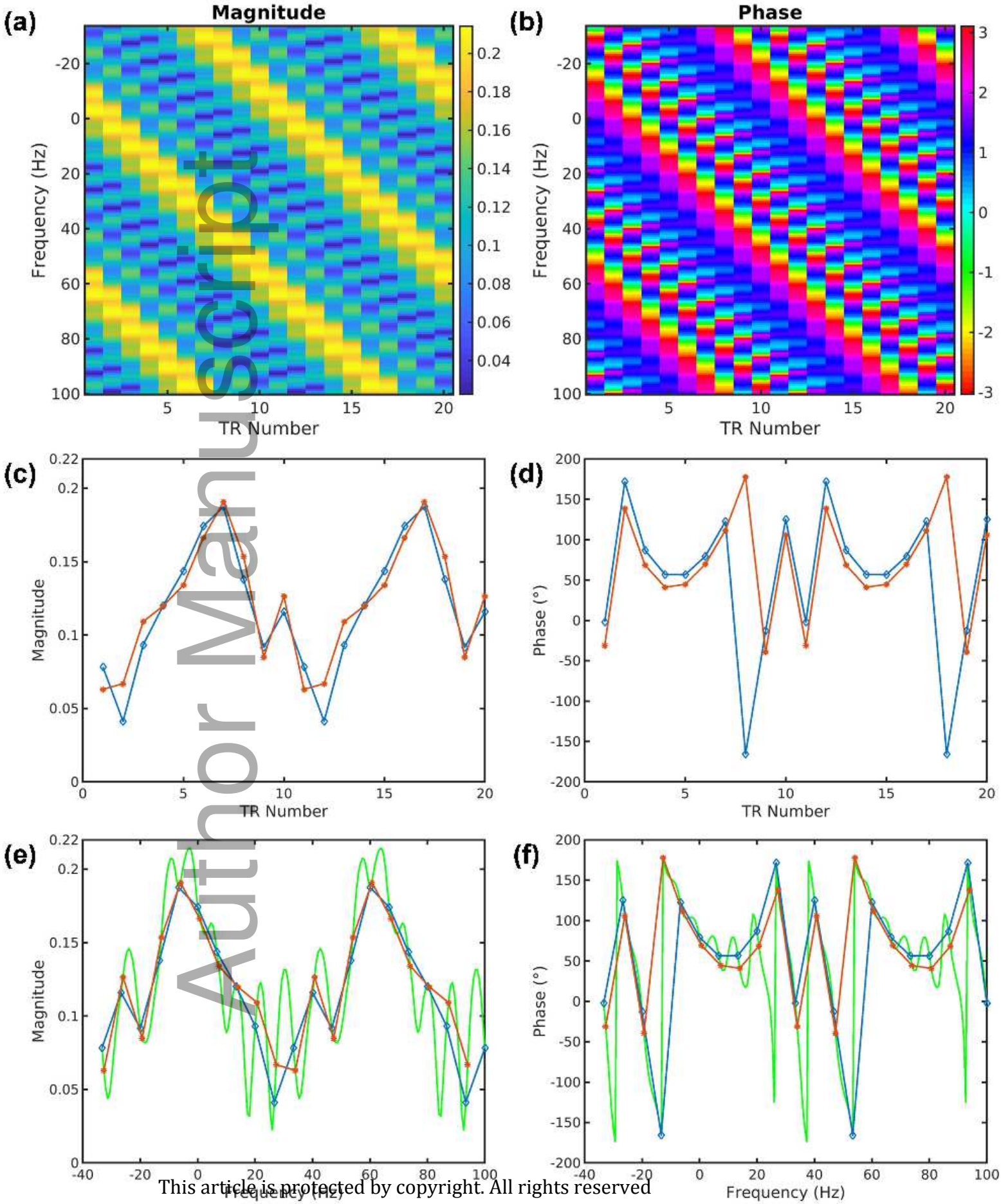

mrm_28156_f2.eps

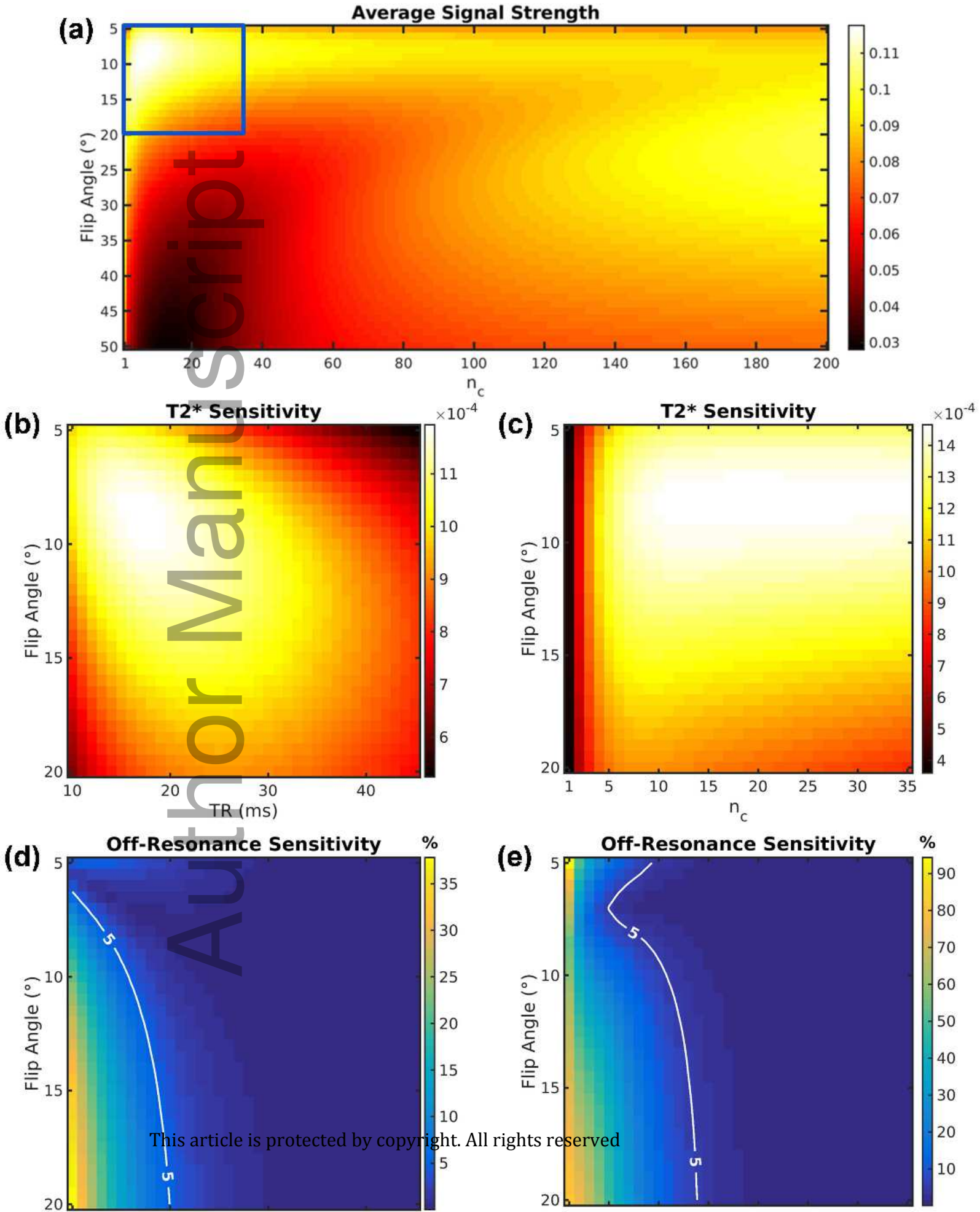

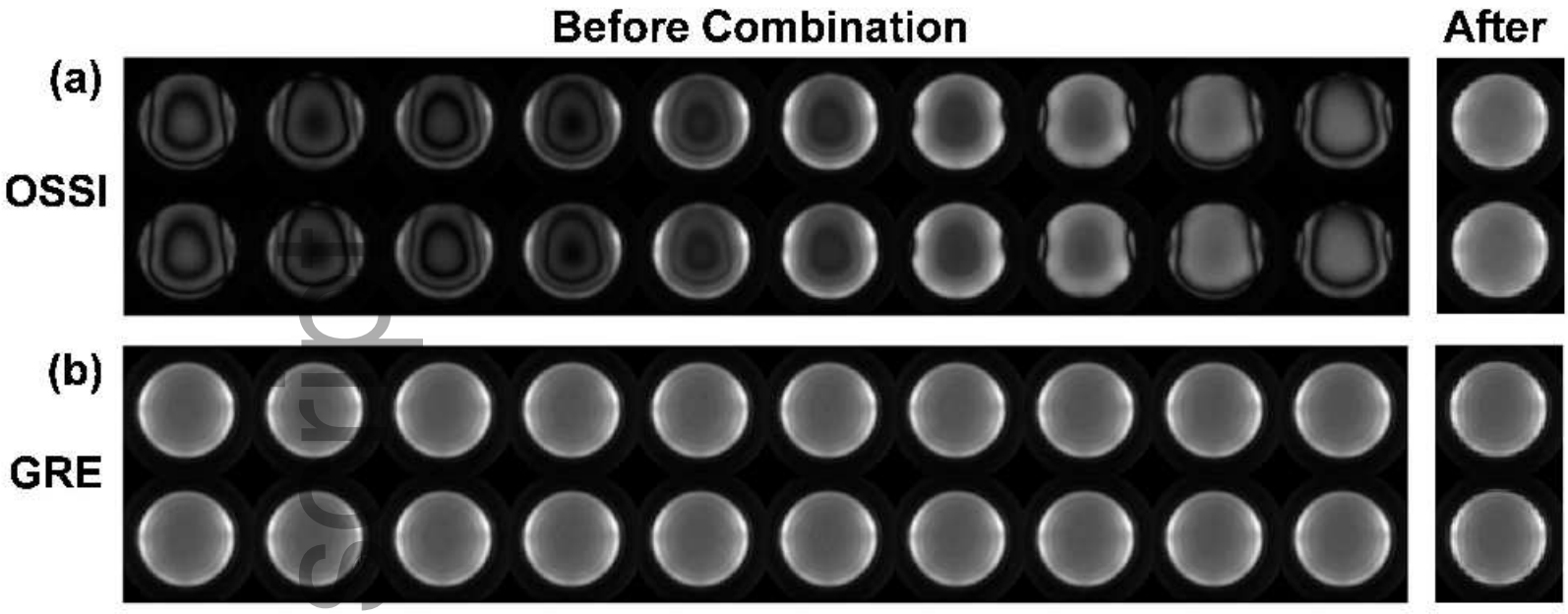

mrm_28156_f4.eps

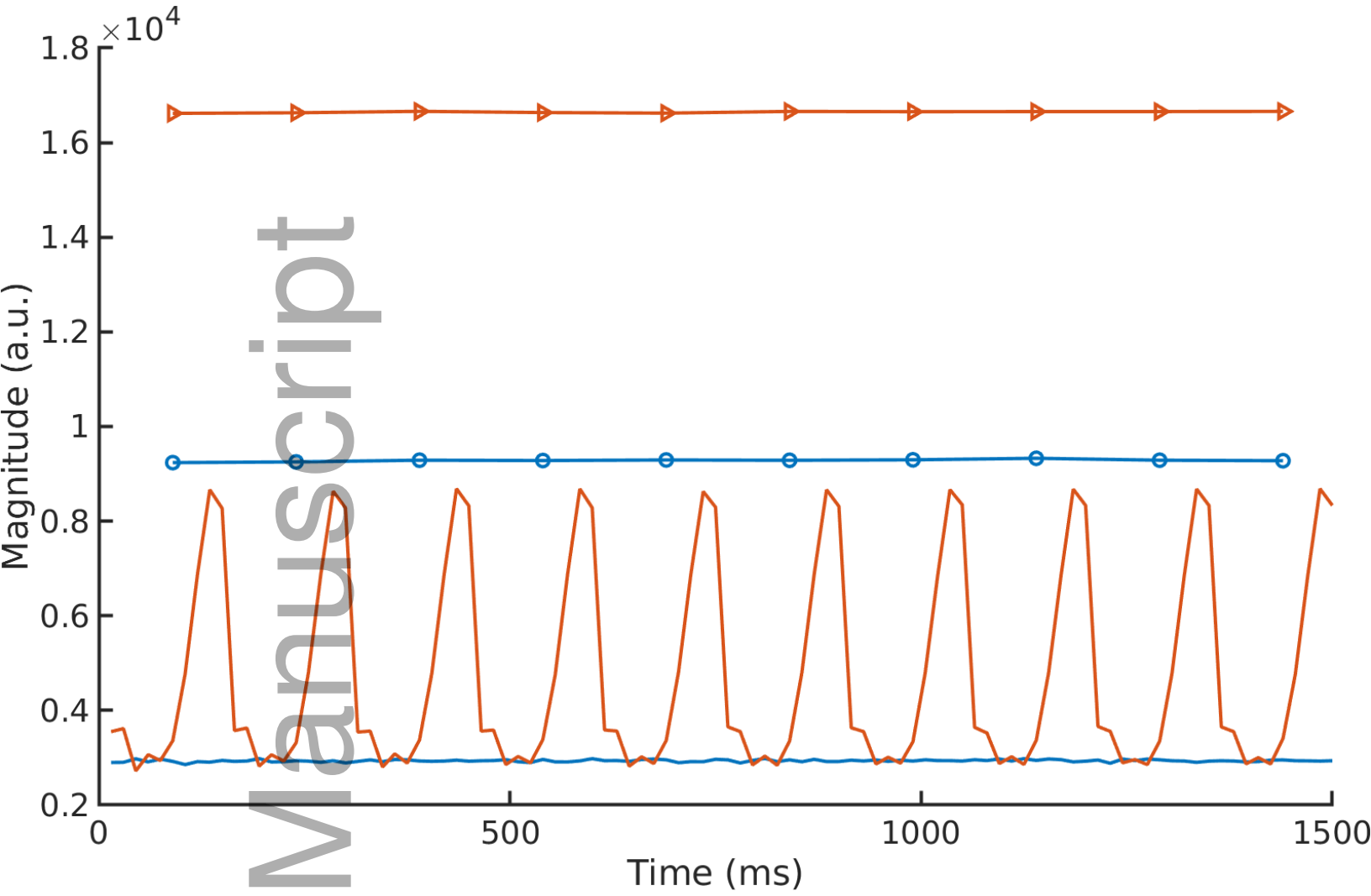

mrm_28156_f5.eps

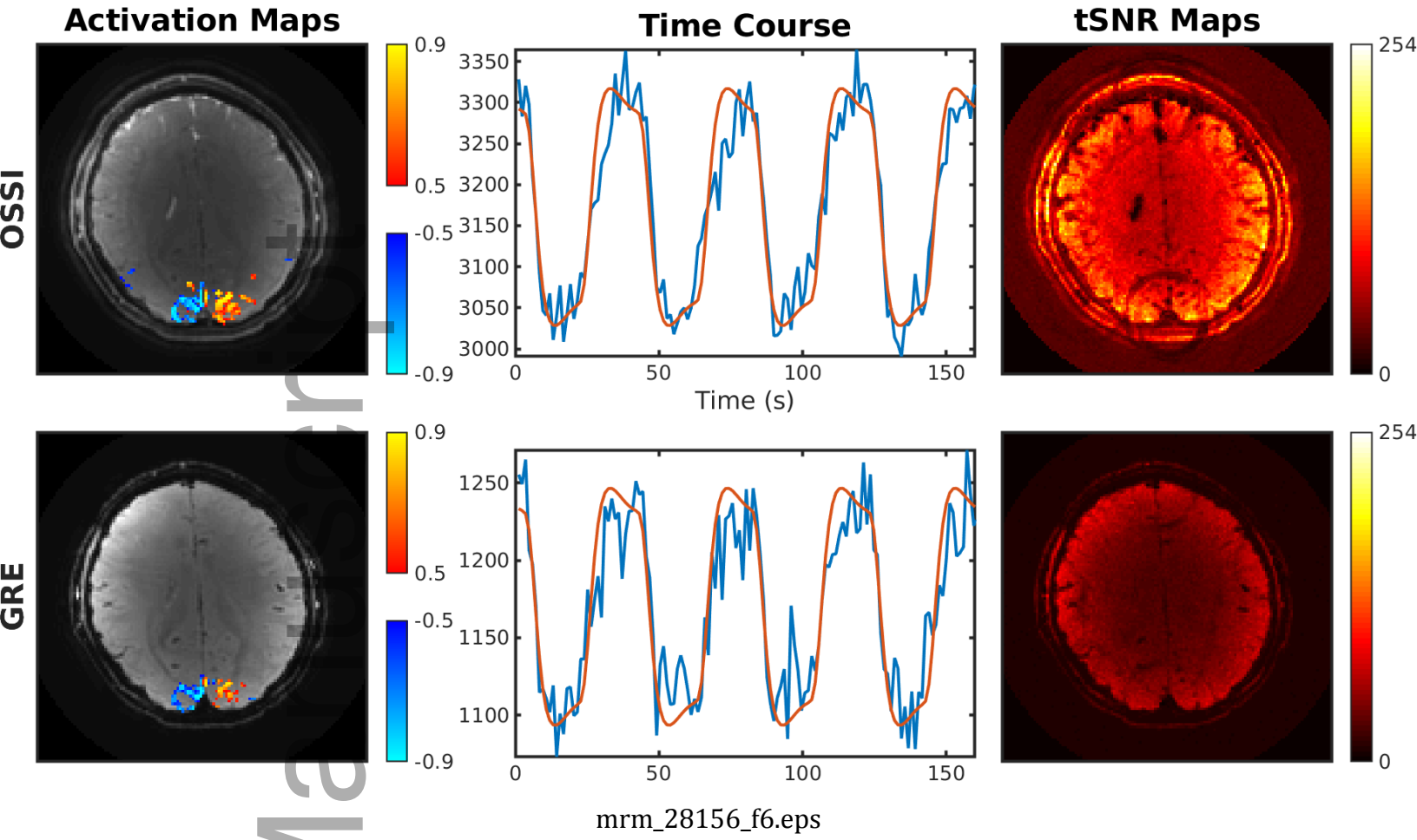

mrm_28156_f6.eps

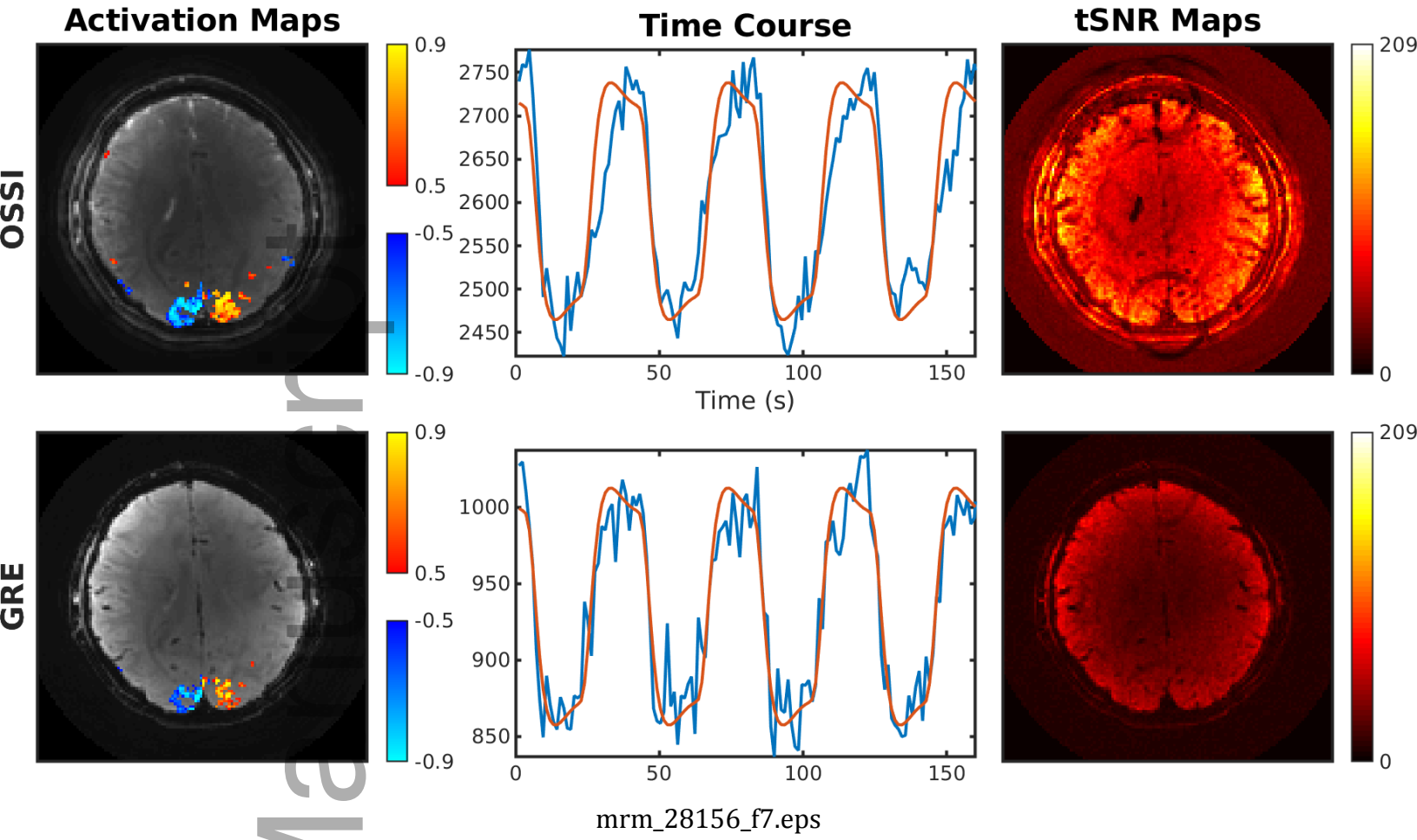

mrm_28156_f7.eps

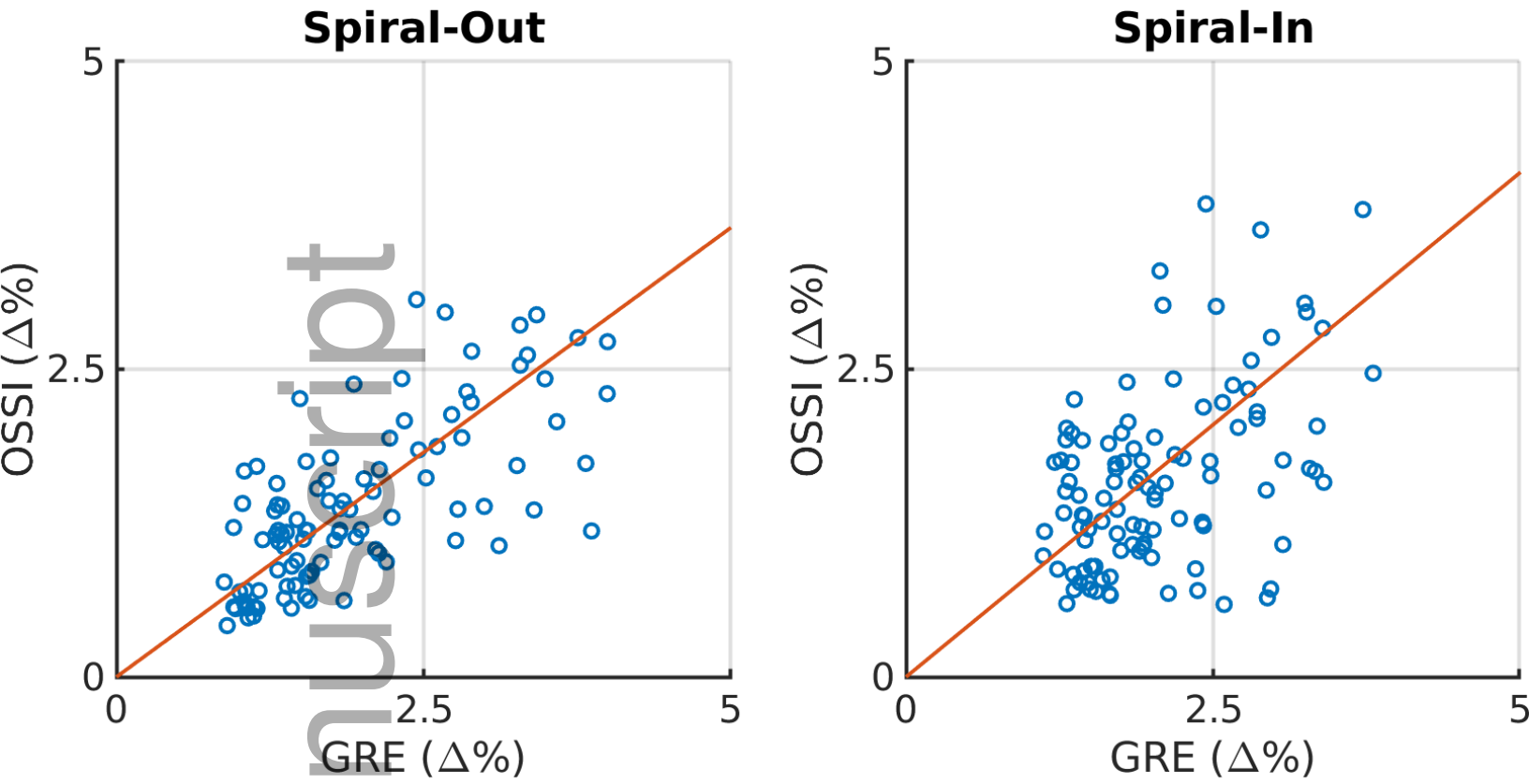

mrm_28156_f8.eps

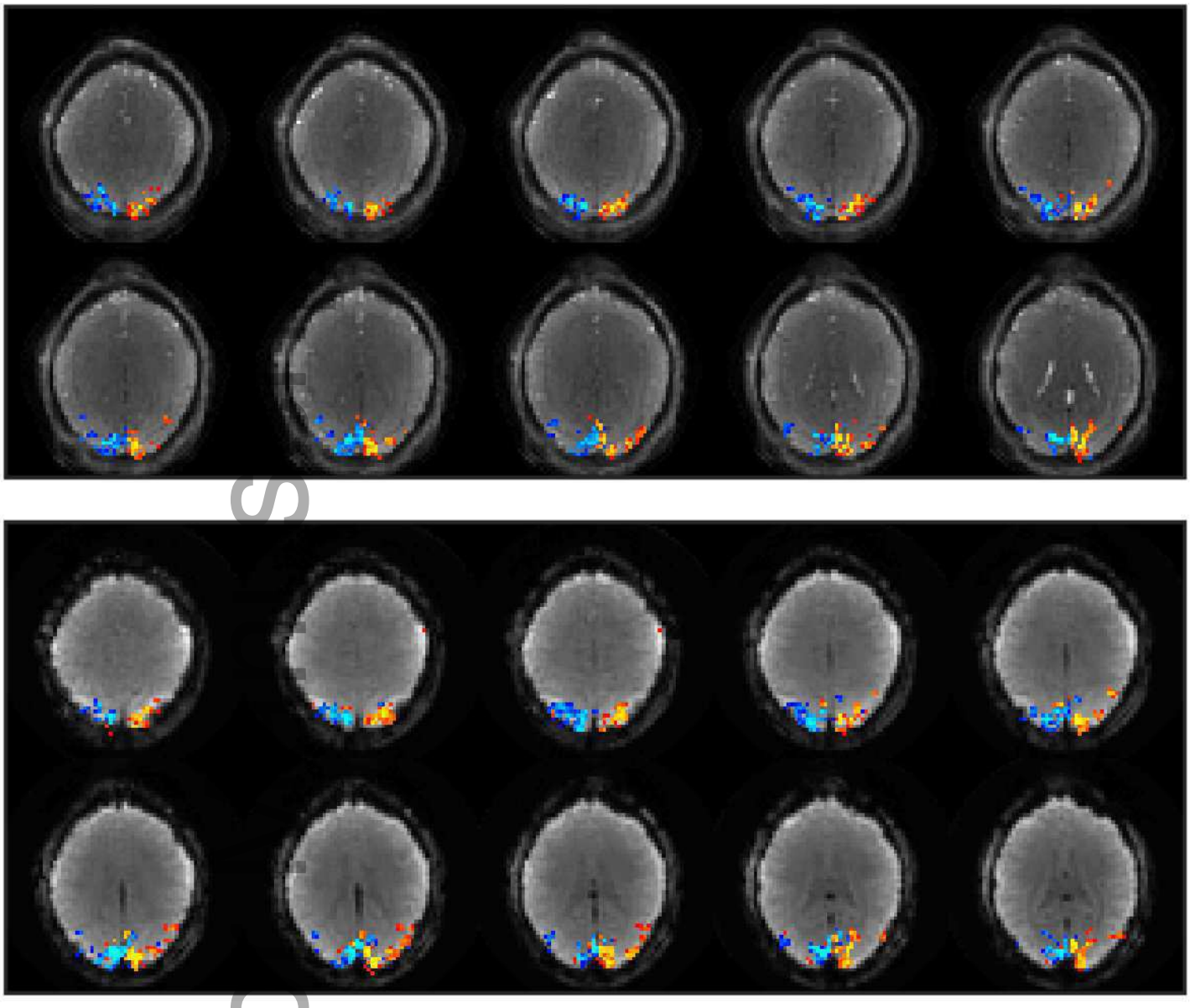

mrm_28156_f9.eps